NANOPARTICLES REMOVAL IN POST-CMP (CHEMICAL-MECHANICAL POLISHING) CLEANING

A Thesis

by

DEDY NG

Submitted to the Office of Graduate Studies of
Texas A&M University
in partial fulfillment of the requirements for the degree of

MASTER OF SCIENCE

August 2005

Major Subject: Mechanical Engineering

NANOPARTICLES REMOVAL IN POST-CMP (CHEMICAL-MECHANICAL POLISHING) CLEANING

A Thesis

by

DEDY NG

Submitted to the Office of Graduate Studies of
Texas A&M University
in partial fulfillment of the requirements for the degree of

MASTER OF SCIENCE

Approved by:

Chair of Committee,	Hong Liang
Committee Members,	Richard B. Griffin
	Ibrahim Karaman
	David W. Goodman
Head of Department,	Dennis O' Neal

August 2005

Major Subject: Mechanical Engineering

ABSTRACT

Nanoparticles Removal in Post-CMP (Chemical Mechanical Polishing) Cleaning.

(August 2005)

Dedy Ng, B.S., The University of Texas at Austin

Chair of Advisory Committee: Dr. Hong Liang

Research was performed to study the particle adhesion on the wafer surface after the chemical-mechanical polishing (CMP) process. The embedded particles can be abrasive particles from the slurry, debris from pad material, and particles of film being polished. Different methods of particle removal mechanism were investigated in order to find out the most effective technique. In post-CMP cleaning, surfactant was added in the solution. Results were compared with cleaning without surfactant and showed that cleaning was more effective with the combined interaction of the mechanical effort from the brush sweeping and the chemistry of the surfactant in the solution (i.e., tribochemical interaction). Numerical analysis was also performed to predict the particle removal rate with the addition of surfactants. The van der Waals forces present in the wafer-particle interface were calculated in order to find the energy required to remove the particle. Finally, the adhesion process was studied by modeling the van der Waals force as a function of separation distance between the particle and the surface. The successful adaptation of elasticity theory to nanoparticle-surface interaction brought insight into CMP cleaning mechanisms. The model tells us that it is not always the case that as the separation distance is decreased, the attraction force will be increased. The force value estimated can be used for slurry design and CMP process estimation.

TO MY PARENTS, MY BROTHER, AND MY DEAREST FRIEND, SENI:

FOR THE LOVE, SUPPORT, ENCOURAGEMENT, GUIDANCE AND FOR

HELPING TO MAKE MY DREAM A REALITY

ACKNOWLEDGEMENTS

The author is grateful to Dr. Hong Liang for her guidance, patience, and endless support. Dr. Liang showed the author that true success comes from hard work and personal initiative. Dr. Liang also provided a great environment to assist the author to work more independently. The author also would like to thank his committee members, Dr. Richard Griffin, Dr. Ibrahim Karaman, and Dr. Wayne Goodman, for their commitment in this research.

The author wishes to thank Dr. Michael Bevan, Dr. Daniel Shantz, and Dr. Maria Barrufet, for their time and assistance in this project. A particular thanks is given to Dr. Andreas Holzenburg for giving invaluable advice and moral support. The author also appreciates Dr. Joseph Reibenspies for his assistance in small angle x-ray scattering (SAXS).

The author wishes to thank his fellow graduate students in the Surface Science Group for their helpful suggestions and the privilege of working together.

Finally, the author would like to thank the friends and family who have supported him through these academic years with care, patience and understanding. Special thanks are extended to the author's parents, for taking the responsibility of instilling since childhood, their belief in the importance of education.

TABLE OF CONTENTS

Page

ABSTRACT iii

DEDICATION iv

ACKNOWLEDGEMENTS v

TABLE OF CONTENTS vi

LIST OF FIGURES viii

LIST OF TABLES x

CHAPTER

I INTRODUCTION 1

1.1. Background 1
1.1.1. Chemical mechanical polishing (CMP) 2
1.1.2. Post-CMP cleaning 4
1.2. Objectives of research 5

II LITERATURE REVIEW 6

2.1. Adhesion theory based on contact mechanics approach 6
2.2. Adhesion theory based on van der Waals and electrostatic dual layer forces 9
2.3. Surfactant in solution 9

III NANOPARTICLES REMOVAL MECHANISMS IN POST-CMP CLEANING 12

3.1. Introduction 12
3.2. Experiments 13
3.3. Theoretical modeling 15
3.3.1. Real contact area between polishing interfaces 15
3.3.2. Contact force and contact area of single effective abrasive particle 16
3.4. Results and discussion 18
3.4.1. Friction force analysis during polishing 18
3.4.2. Cleaning results 21
3.4.3. Adhesion force and energy required to remove one particle 25
3.4.4. Removal mechanisms during post-CMP cleaning 25
3.4.5. Friction analyses in post-CMP cleaning 26
3.5. Conclusions 27

CHAPTER Page

IV ROLE OF SURFACTANT MOLECULES DURING POST CMP-CLEANING 28

4.1. Introduction 28
4.2. Experiments 30
4.3. Results and discussion 31
4.3.1. Friction analyses in post-CMP cleaning 31
4.3.2. Micelles formation in cleaning solution 33
4.3.3. Surface tension of the clean surface 36
4.3.4. Surface topography of the clean surface 37
4.4. Conclusions 38

V MODELING OF ADHESIVE FORCES ON ELASTIC SURFACES-AN ELASTICITY THEORY APPROACH 39

5.1. Introduction 39
5.2. Analysis 41
5.2.1. van der Waals force expression 41
5.2.2. Expression for the deformation at the mid-point of a surface . 43
5.2.2.1. Uniformly distributed vertical loading of a straight boundary 43
5.2.2.2. Vertical displacement at the mid-point 46
5.2.2.3. Outline of the procedure 47
5.2.2.4. Definition of ALPHA 47
5.2.2.5. Definition of error % 47
5.3. Results and discussion 50
5.4. Conclusions 55

VI CONCLUSIONS AND RECOMMENDATIONS 56

6.1. Conclusions 56
6.2. Recommendations for future work 56

NOMENCLATURE 58

REFERENCES 62

VITA 66

LIST OF FIGURES

FIGURE		Page
1	Industrial CMP setup	3
2	Post-CMP cleaning setup	5
3	Schematic drawing of Hertzian deformation of a sphere	6
4	Schematic drawing of DMT and JKR adhesion model	7
5	Plot of surface tension vs. surfactant concentration in aqueous solution	10
6	Surfactant molecules behavior below CMC (a), and above CMC (b and c)	11
7	Schematic drawing of polishing setup	14
8	Schematic drawing of post-CMP cleaning setup	14
9	Schematic view of abrasive particles trapped at top of polishing pad	17
10	Schematic of the embedded particle on the wafer surface	19
11(a)	Different penetration depth can be achieved with different particle size	20
11(b)	Resulting particle friction due to different particle size	21
12	AFM image of cleaned wafer surface with deionized water. The scanned area is 412 μm^2	22
13	AFM image of cleaned surface with surfactant. The scan area is12 μm^2	23
14	Variation of down force for different particle size	24
15	Friction coefficient vs. cleaning time during post-CMP cleaning	26
16	Schematic representation of repulsive barrier due to the formation micelles in the solid-liquid interface	29
17	Small angle x-ray scattering spectroscopy (SAXS)	31
18	Surfactant concentration (%wt) as a function of average friction coefficient.	32
19	Temperature (^{0}C) as a function of average friction coefficient	33
20	The scanning intensity of micelles formation as a function of scattering factor	34
21	The mean radius gyration for 1 %wt concentration	35
22	Schematic diagram of a contact angle, θ measurement	36

FIGURE Page

23 AFM image of silicon surface after post-CMP cleaning with different amounts of surfactant (a) at 0.1 %wt surfactant, (b) at 0.7 %wt surfactant….. 37
24(a) No surface deformation 40
24(b) Surface deformation 40
25 The Lennard-Jones potential 42
26 Schematic drawing of vertical displacement of surface at the mid-point 46
27 Initial force vs. ALPHA 48
28 For an assumed ALPHA equal to 77.71 49
29 %Error vs. ALPHA for an initial ALPHA 50
30 %Error vs. ALPHA for ALPHA =100 51
31 %Error vs. ALPHA for ALPHA =90 51
32 %Error vs. ALPHA for ALPHA =80 52
33 %Error vs. ALPHA for ALPHA =70 53
34 %Error vs. ALPHA for ALPHA =60 53

LIST OF TABLES

TABLE Page

1 Friction force calculation 20
2 A comparison result between post-CMP cleaning with and without surfactant..... 24
3 Mean actual radius of micelle for each surfactant concentration 35
4 Contact angle measurement for the clean surface..... 36
5 Lennard-Jones potential parameters 43
6 Conclusive results from the plotted figures 53

CHAPTER I

INTRODUCTION

1.1. Background

Chemical mechanical polishing (CMP) was introduced as a method to planarize inter-level dielectrics (ILD) and damascene metal wiring for on-chip multi-level interconnects [1-3]. As the size of microelectronic devices to be fabricated get smaller, CMP has become a standard process to greatly enhance the capability of commercial semiconductor processes. Its initial application and subsequent enormous growth to date have attracted great research efforts to understand and optimize this process. During CMP, a wafer is held upside down in a carrier and pressed into contact with a slurry film flowing over a slurry-saturated polishing pad. The surface of wafer is polished both by mechanical abrasion and by chemical erosion in order to achieve local and global planarization. One major concern in CMP is particle adhesion on the substrate surface. These particles can be abrasive particles from the slurry, debris from pad material, and particles of film being polished. Adhesion of these particles to the substrate presents a serious threat to manufacturing productivity. Particle contamination is the major reason for low yield. To achieve a high quality surface, CMP process is followed by a cleaning process which is called post-CMP cleaning. Since CMP utilizes slurry containing abrasive particles to provide mechanical action for surface removal, post-CMP wafers require the removal of any residual slurry by a wet cleaning process. The most widely used cleaning method is a contact cleaning method which involves direct contact between a polymeric brush and the surface substrate. During cleaning, a substrate is immersed in a cleaning solution containing deionized water and come into contact with the brush. To enhance the cleaning process, a surfactant maybe added in the cleaning solution to weaken the adhesion forces that bind the particles to the substrate surface.

This thesis follows the style of the *Journal of Electrochemical Society.*

Surfactant has been added into cleaning solution as an industrial practice. The effects of surfactant in cleaning have not been well reported. Surfactant has two structures: hydrophobic which contains an organic tail group and hydrophilic that has a head group [4]. When surfactant is mixed with deionized water, the molecules will dissolve and form a layer of saturation on the substrate surface. The bond strength of substrates is weakened and will in turn reduce the surface tension. At this level, surfactant can form small colloidal sized particles called micelles, to react with particles on substrate surface by changing the surface charge of substrates.

The motivation of this research is to understand CMP and cleaning further in depth. The approaches in understanding CMP is from a different perspective that has yet been investigated. In order to understand particle removal, we start from the particle adhesion process during CMP. The knowledge of adhesion helps to understand particle removal mechanisms. In the polishing process, we make the following assumptions: the uniform load distribution during CMP process, the uniform distribution on pad asperities, a direct contact between pad and particles, and a direct contact between substrate and particles. For the cleaning process, the method used in this study is a direct contact with the substrate surface through brush sweeping, which uses a tribological approach over a range of surfactant concentration and temperature. To enhance the cleaning process, an anionic surfactant containing alcohol ether sulfate (AES) will be added in the cleaning solution. Our previous research has shown that hydrodynamic force is limited for effective cleaning [5,6]. Therefore, in this work we focus on the direct contact force.

1.1.1. Chemical mechanical polishing (CMP)

CMP was originally used for glass and silicon wafer polishing. As its functionality increases, CMP is being introduced in planarizing the interlayer dielectrics (ILD), shallow trench isolation (STI) and damascene metal wiring for on-chip multi-level interconnects [1-3]. This process has been adapted to copper (Cu), tungsten (W)

and low k dielectric in the semiconductor processing. The goal of CMP is to achieve planarization of rough surfaces.

During the CMP process, a wafer is held upside down in a carrier and pressed into contact with slurry film flowing over a slurry-saturated polishing pad (Figure 1).

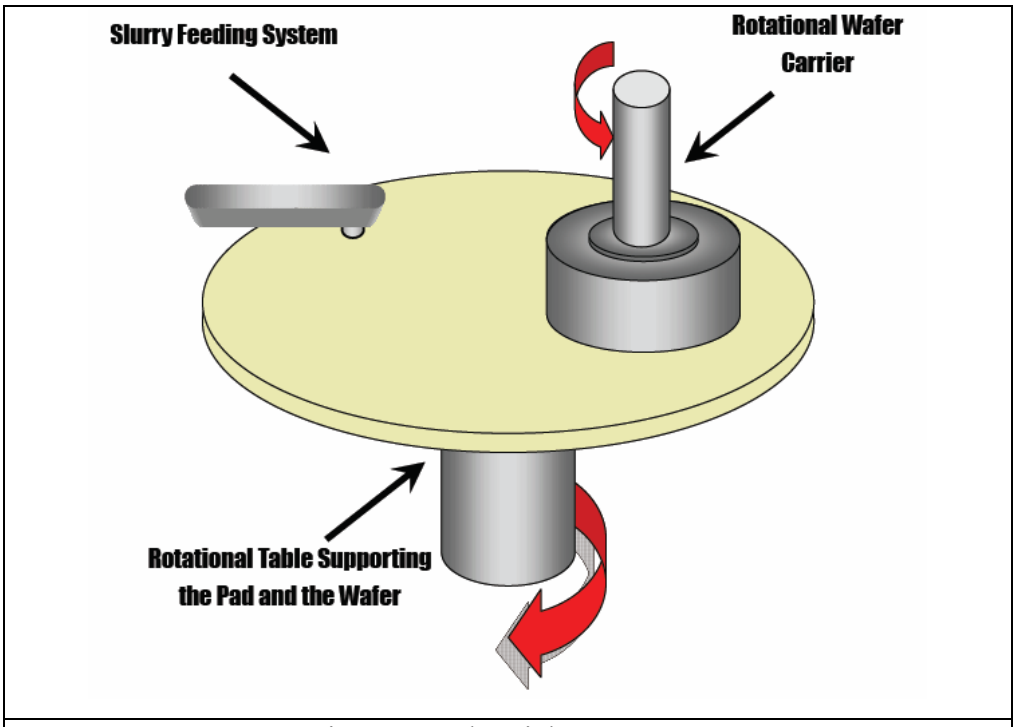

Figure 1. Industrial CMP setup

The surface of wafer is polished by both mechanical abrasion and chemical erosion, in order to achieve local and global planarization. This process is crucial in preparing a smooth layer of surface so that subsequent processes can begin from a flat surface.

As new generations of chips become increasingly smaller, below 0.13 micron, CMP plays a critical role in maintaining a wafer's integrity [7]. With CMP, high-performance and more reliable chips at a lower cost of ownership can be achieved by

expanding the volume of the integrated circuit (IC) fabrication. The knowledge on CMP technology is crucial in optimizing the IC design and manufacturing.

1.1.2. Post-CMP cleaning

Post-CMP cleaning is a follow up process after the initial CMP. Post-CMP cleaning is required to remove surface contamination. During polishing, wafer surface exposed to the slurry solution and pressed against the interfaces may be contaminated with slurry particles, trace metals, debris from pad material and/or mobile ions. The resulting process may cause a subsurface damage on the surface that can adversely affect device properties. However, a greater concern is the substantial and unavoidable levels of surface contaminations. These remaining contaminants can cause patterning or deposition errors in subsequent process. In the greater scale, these contaminations can potentially reduce device yields and cause a serious threat to the manufacturing productivity.

There are two cleaning methods used in post-CMP cleaning, which are non-contact and direct contact methods. The non-contact cleaning method uses a hydrodynamic drag approach where particles are removed from the surface by viscous drag forces developed in the fluid and issues such as the thickness of the boundary layer film are limiting factors in particle removal and cleaning efficiency [6]. As for the direct contact method, a double-sided brush which comes into a contact with the surface is employed together with the hydrodynamic drag in the fluid for particle removal (Figure 2).

During cleaning, a surfactant or other solution chemistry may be added to the cleaning solution. The solution chemistry plays an important role in the cleaning effect. The pronounced effect of this cleaning solution will be covered in details in Chapter 3.

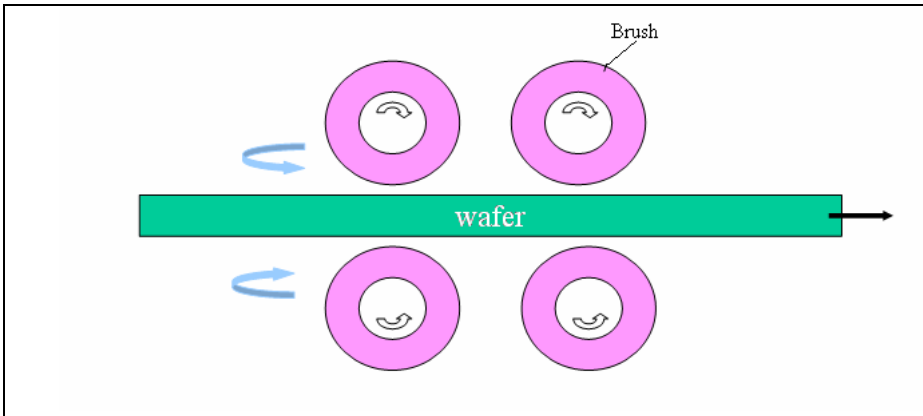

Figure 2. Post-CMP cleaning setup

1.2. Objectives of research

The main objective of this research is to study the particle removal mechanism in the post-CMP Cleaning. Three methods are employed in approaching this study. The first is to perform cleaning by brush sweeping method, then the addition of chemical and additives in the cleaning solution, and finally by numerical modeling to predict the adhesion force range and the deflected surface.

As for the characterization tools, micelles formations were characterized by small angle x-ray scattering spectroscope (SAXS), the surface topography can be carried out by using atomic force microscope (AFM) and scanning electron microscope (SEM). Surface tension of surfactant in liquid interface can be observed by using surface tensiometer. Contact angle between a droplet of deionized water and the clean surface can be measured using a CCD camera.

CHAPTER II

LITERATURE REVIEW

2.1. Adhesion theory based on contact mechanics approach

Hertzian theory is the first model to study the elastic deformation on surface without considering the effect of adhesion [8]. This theory considers a sphere with applied load on the elastic surface as shown in Figure 3.

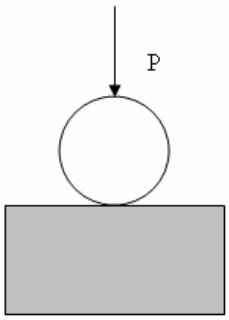

Figure 3. Schematic drawing of Hertzian deformation of a sphere

The relationship is given by:

$$P = \frac{4Ea^3}{3R} \tag{1}$$

where P is the applied load, E is the elastic modulus, a is the contact radius and R is the radius of the sphere.

Dejarguin-Muller-Toporov (DMT) modified the Hertzian theory to explain the adhesion model for elastic deformation [9,10]. They derived a solution for a sphere contacting a hard solid surface with small radius which accounts for adhesion forces just outside the contact circle only when contact occurs as shown in Figure 4.

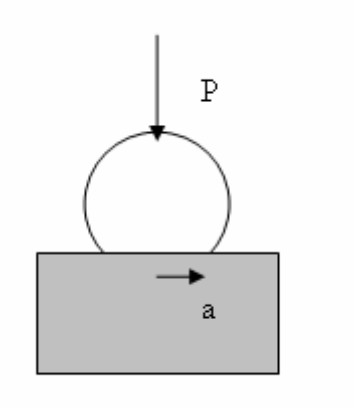

Figure 4. Schematic drawing of DMT and JKR adhesion model

Compared to Hertzian contact areas, DMT contact areas are larger which lead to the introduction of van der Waal's forces. The DMT model gives the contact radius, a, related to the work of adhesion, $\Delta\gamma$, by:

$$a^3 = \frac{R}{K}\left(P + 2\pi\Delta\gamma R\right) \tag{2}$$

where R is the radius of the sphere, P is the applied load, K is the composite Young's modulus, which equation is given by $\frac{4}{3}\left(\frac{1-\upsilon_1^2}{E_1}+\frac{1-\upsilon_2^2}{E_2}\right)^{-1}$ (3)

, where υ is the Poisson's ratio and E is the elastic modulus.

It is obvious that upon application of a negative load, P_c is given by:

$$P_c = -2\pi\Delta\gamma R \tag{4}$$

and the contact radius is zero, which means the two surfaces separate at that point. Therefore, P_c is the critical force required to separate the two spheres, i.e. the pull-off force. The model also gives a particular value for the contact radius at a zero load, a_0 as:

$$a_0 = (2\pi\Delta\gamma R^2 / K)^{1/3} \tag{5}$$

Johnson-Kendall-Roberts (JKR) theory is a continuum mechanics model of contact between two solid spheres [11]. It accounts for adhesion forces within the expanded area of contact only and is applicable to large radius, compliant solids. The JKR theory is a revision of Hertzian contact theory and results in the additional increase in the contact area between soft elastomeric hemispheres to adhesive forces between the two surfaces. The JKR theory does estimate the surface free energy of the interface and the work of adhesion (W_a) between solids.

Considering the effect of adhesion force on the deformation of an elastic sphere in contact to an elastic half space, the contact radius, a is given by:

$$a^3 = \frac{D}{2K}\left[P + \frac{3}{2}W_a \pi D + \sqrt{3\pi W_a DP + \left(\frac{3\pi W_a D}{2}\right)^2}\right] \tag{6}$$

where d is the diameter of a sphere, W_a is the thermodynamic work of adhesion, P is the downward load applied to the top surface of the sphere and K is the composite Young's modulus given at equation (3).

In the absence of surface forces, $W_A = 0$ and the equation is reduced to the classical Hertz model, which is

$$a^3 = \frac{DP}{2K} \tag{7}$$

Maugis and Pollock (MP) generalized an adhesion model for plastic deformation by assuming that the contact area can be determined by the hardness of the deformed material [12-14]. As either the externally applied load or the adhesion force increases, the deformation takes place from elastic to elastoplastic and lastly to fully plastic. Although no theory of particle adhesion exists for the elastoplastic regime, when the deformation is fully plastic,

$$P + 2\pi W_a = 3\pi a^2 Y \tag{8}$$

where Y is the yield strength of the yielding material and is related to the material's hardness, m, by

$$m = 3Y \tag{9}$$

2.2. Adhesion theory based on van der Waals and electrostatic dual layer forces

The Dejarguin, Landau, Verwey, and Overbeek (DLVO) theory describes the adhesion of particles on the surface was due to the effect of van der Waals and electrical dual layer forces [15,16]. The total adhesion force on the surface can be written as:

$$F_t = F_{vdw} + F_{edl} \tag{10}$$

where F_t is total adhesion force, F_{vdw} is the van der Waals force, and F_{edl} is the electrical dual layer force.

Furthermore, when the particles come in contact with the surface, a certain amount deformation might occur at the interface, this will increase the adhesion force between the particle and surface. To account for this deformation, the van der Waals force is broken into two components, the force acting on the interface before the deformation and the force acting on the contact area due to deformation. Thus the van der Waals can be written as:

$$F_{vdw} = \frac{AD}{12r^2}\left(1 + \frac{2a^2}{hD}\right) \tag{11}$$

where A is the Hamaker constant, D is the diameter of the particle, r is the separation distance between the particle and surface, and a is the contact radius of the particle and surface. For elastic deformation, the JKR or the DMT theory can be used to find the contact radius. For plastic deformation, the MP theory is used to calculate the contact radius.

2.3. Surfactant in solution

Surfactant molecules are water-soluble surface-active agents comprising of a hydrophobic (water fearing) and hydrophilic component (water loving). Depending on the nature of the charge present in the hydrophilic portion, surfactants are classified as: anionic, cationic, zwitterionic, and nonionic. For zwitterionic the surface-active portion bears both positive and negative charge, whereas the cationic and anionic the surface-active portion bear a positive charge and negative charge, respectively. For nonionic, the surface-active bears no ionic charge.

Generally, surfactants possess the ability to lower the surface tension when mixed with water, as illustrated in Figure 5. The characteristic discontinuity in the plots of surface tension against surfactant concentration can be measured by using surface tensiometer. The corresponding surfactant concentration at this discontinuity is referred as critical micelle concentration (CMC). In other word, critical micelle concentration (CMC) is a measure of the concentration of a solution component which represents a critical value above. Ultimately, it increases the concentration of that component forces formation of micelles.

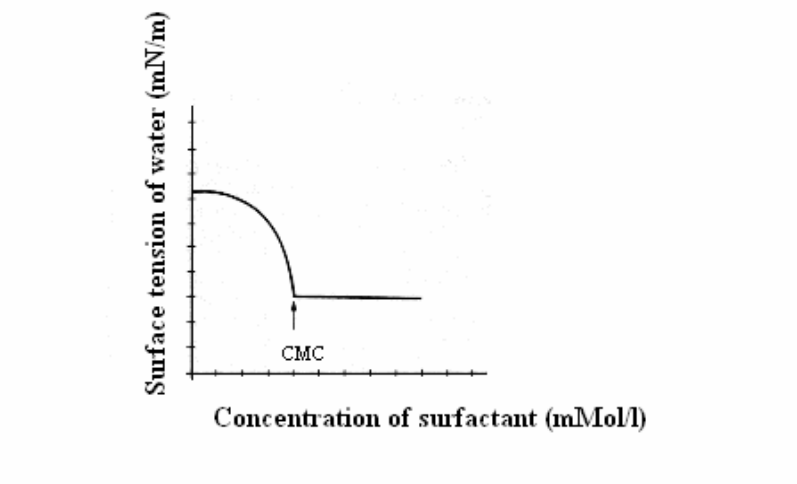

Figure 5. Plot of surface tension vs. surfactant concentration in aqueous solution

At surfactant concentrations below the CMC, the surfactant molecules are loosely integrated into the water structure, which is also known as monomer (a) is illustrated in Figure 6. At the concentration above the CMC, the surfactant-water structure will alter according to the surfactant molecules. This is due to the fact that the surfactant molecules will begin to build up their own structures micelles in the interior (b) or form monolayers at the surface (c).

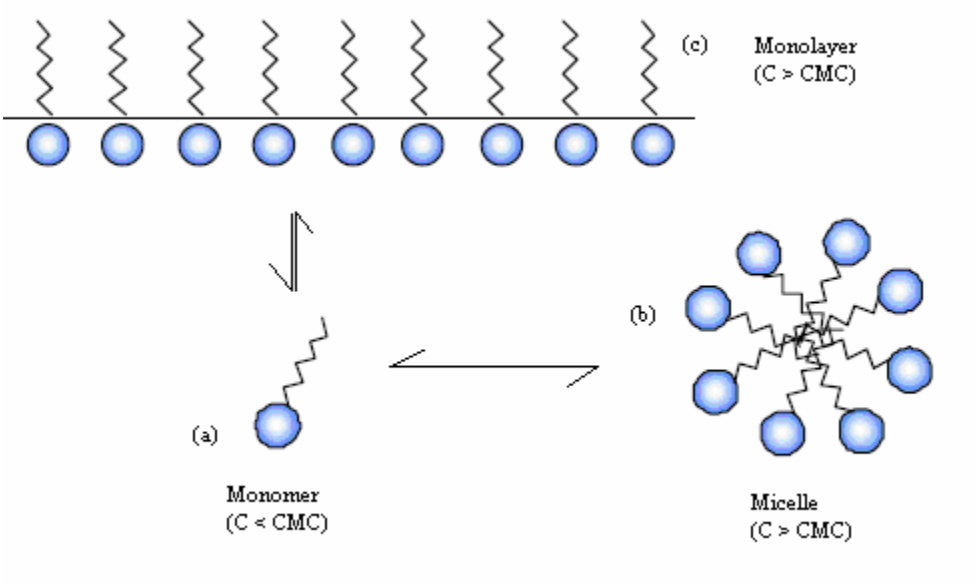

Figure 6. Surfactant molecules behavior below CMC (a), and above CMC (b and c)

Aggregates are observed in which the hydrophobic or hydrophilic portion of the surfactant are fixed together because of the limited solubility of surfactants in water [17]. The micelle may be represented as a globular cylindrical orellipsoidal cluster [18] of individual surfactant molecules in equilibrium with its monomers [17-29]. Moreover, the reverse orientation of the two component of the surfactant in a hydrocarbon medium can lead to a reversed micelles structure [30]. Planar bilayers or small unilamellar vesicles are also observed [31].

CHAPTER III

NANOPARTICLES REMOVAL MECHANISMS IN POST-CMP CLEANING

3.1. Introduction

As the size of microelectronic device dimensions decreases, planarization of both front and back end layers is crucial for technologies smaller than 0.5 μm [32]. The CMP processes leave a large amount of contamination on the surface such as residual particles, metallic contamination and even a damaged layer on the surface. Therefore a new cleaning process must be introduced after the CMP process called post-CMP cleaning. The major concerns on the CMP are the high level of residual particles. Depending on the type of CMP and the polishing conditions, these particles can be physically adsorbed at the surface or partially embedded in the substrate due to the mechanical pressure exerted by the polishing pad.

Since the van der Waals force is more dominant in the adhesion process, it must be overcome by using the mechanical effort from the brush scrubbing or by using chemical solution or additives. In the case of fine particles, the mechanical effort will not be sufficient. Thus the chemical or additives must be added to control the electrostatic repulsion in order to prevent particle readhesion. This can be done by controlling the charges on the substrate and particles, which can be altered by modifying the solution pH or the addition of surfactant. The novel idea of using surfactant is that it can be used to modify the apparent charges on particle and substrate surface. Another important characteristic is that particles can be kept apart during the occupation of the organic surfactant molecules when attached to the particle.

CMP and post-CMP cleaning are standard processes for local and global planarization. Researchers have attempted to approach them from different point of views in accordance to their needs. For example, Burdick et al. used a theoretical evaluation of hydrodynamic force effect on particle removal in post-CMP cleaning [33,34]. Zhang et al. tried to see the effect of using brush and spin-rinse drying in order

to study the particle removal during post-CMP cleaning [35]. Cooper et al. investigated the particle removal by modeling the adhesive force [36-39]. In another experiment that they have done, Cooper and co-authors tried to use several type of cleaning solution to study the adhesion process [40]. Eichenlaub et al. focused on simulation of slurry particles removal [41] and surface roughness to study the adhesion process [42]. Zhang et al. created a model to study the removal force from buffing and brushing during post-CMP cleaning [43]. Hong et al. studied the effect of additives in particle adhesion and removal [44]. Estragnat et al. studied the tribological behavior of silicon CMP [5] and lubrication performance during post-CMP cleaning [6]. Zhang et al. modified the slurry chemistry to minimize defects during CMP and post-CMP cleaning [45]. These results, among others, have discussed the mechanical nature of surface material removal in a micrometer length scale and larger. The abrasive particles used in CMP are in nanometer. Interesting questions arose when sizes considered become smaller.

In previous research we found that hydrodynamic force is limited for effective cleaning [5,6]. Therefore, in this work we will focus on the direct contact force in order to see the effectiveness of the particle removal. The affect of surfactant in reducing this contact force will be discussed.

3.2. Experiments

The first step in this experiment is to polish sample materials. The slurry solution was made by mixing 50 mL deionized water and 0.5 g fumed silica particles that were obtained from Cabot Microelectronics. The polishing pad used was made of polyurethane (Rodel 1000), where the pad was conditioned for more than 2 hours. During polishing experiments, ten 1.6 cm x 1.6 cm silicon wafers were polished with the Buehler tabletop polisher. The polishing was conducted at room temperature. The applied pressure used was 17 kPa and the polishing platen rotated at a constant speed of 10 cm/s for 30 minutes. The schematic drawing of polishing setup is shown in Figure 7.

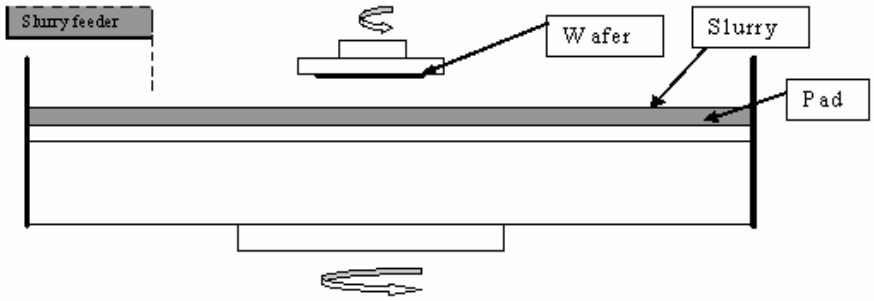

Figure 7. Schematic drawing of polishing setup

The cleaning experiments were performed on a disk-on-disk tribometer (CSM). Figure 8 shows the schematic for the cleaning set-up.

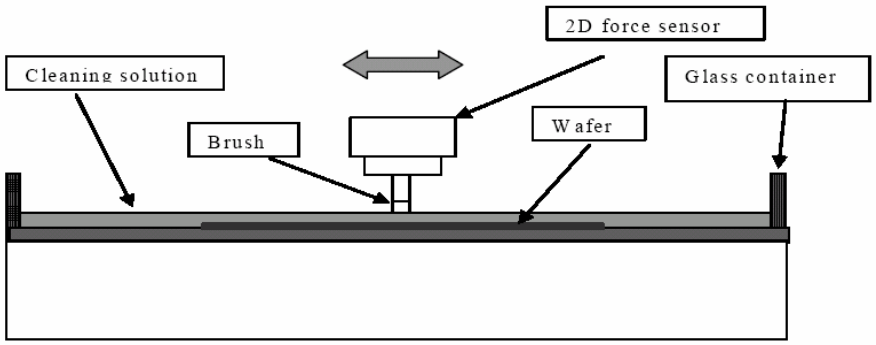

Figure 8. Schematic drawing of post-CMP cleaning setup

The brush was used as the upper disk and the wafer was the lower one. The polyvinyl alcohol (PVA) brush (Rippey) was used for this study. Two cleaning solutions were prepared for this experiment. In the first solution, 10 mL deionized water was used as a cleaning solution. The second solution was made by mixing 10 mL deionized water and 0.1 wt % anionic surfactant containing alcohol ether sulfates (AES). Prior to data acquisition, the brush, 5 mm in diameter, was soaked in deionized water for

30 minutes. The cleaning experiment was performed at room temperature with the following parameter: the brush pressure was 125 Pa and the speed was 0.5 cm/s. The brush moved in a reciprocating at seven locations across the wafer. Following the cleaning process, the sample was cleaned with deionized water in an ultrasonic cleaner for 1 minute to prevent redeposition of particles to the substrate.

3.3. Theoretical modeling

As mentioned earlier, in order to understand particle removal mechanisms, it is important to know how particles are adhered to wafer surfaces during polishing. The numerical modeling here is to illustrate how particles are adhered to wafer surface under different loading conditions.

3.3.1. Real contact area between polishing interfaces

In the current model, the contact area between the polishing interfaces is calculated using a micro-contact model for the pad and wafer surface that considers the elastic, elastoplastic, and plastic deformations of the polishing pad asperities [46]. Substituting the polishing pad and wafer parameters into the micro-contact model gives the contact area between the CMP interfaces as:

$$\begin{aligned}\frac{A_r}{A_n} &= \eta\cdot\pi\cdot R_a\cdot\int_d^{d+\omega_e}(z-d)\cdot\varphi(z)\,dz \\ &+2\cdot\eta\cdot\pi\cdot R_a\cdot\int_{d+\omega_p}^{\infty}(z-d)\cdot\varphi(z)\,dz \\ &+\eta\cdot\pi\cdot R_a\cdot\int_{d+\omega_e}^{d+\omega_p}(z-d)\cdot\left[1-2\left(\frac{\omega-\omega_e}{\omega_p-\omega_e}\right)^3+3\left(\frac{\omega-\omega_e}{\omega_p-\omega_e}\right)^2\right]\cdot\varphi(z)\,dz\end{aligned} \tag{12}$$

where the A_r is the total real contact area of polishing interface, A_n is the nominal contact area of polishing interface, η is the area density of asperities , R is the average radius of the asperities, z is the height of asperity measured from the mean of asperity heights, d is the distance between the rigid flat surface of the wafer and the mean plane of the pad asperities, $\varphi(z)$ is the distribution function of the asperity heights, and ω, ω_e

and ω_p are the interference, critical interference at the point of initial yielding of the asperity, and critical interference at the point of fully plastic flow, respectively. Furthermore, the contact force at the polishing interface can be calculated from:

$$\frac{F_r}{A_n \cdot E'} = \frac{4}{3} \cdot \eta \cdot R_a^{1/2} \cdot \int_d^{d+\omega} (z-d)^{3/2} \cdot \varphi(z)\, dz + \eta \cdot \pi \cdot \frac{H_p}{E'} \cdot \int_{d+\omega_e}^{d+\omega_p} \left[1 - 1\left((1-k) \cdot \frac{\ln \omega_p - \ln \omega - \ln 2}{\ln \omega_p - \ln \omega_e} \right) \right] \cdot \left[1 - 2\left(\frac{\omega - \omega_e}{\omega_p - \omega_e} \right)^3 + 3\left(\frac{\omega - \omega_e}{\omega_p - \omega_e} \right)^2 \right] \cdot (z-d) \cdot \varphi(z)\, dz + 2 \cdot \pi \cdot \eta \cdot R_a \cdot \frac{H_p}{E'} \cdot \int_{d+\omega_p}^{\infty} (z-d) \cdot \varphi(z) dz \tag{13}$$

where F_r is the contact force at the polishing interface, E' is the equivalent Young's modules for the contact surfaces H_p is the hardness of the polishing pad material, k is the mean contact pressure factor.

It should be noted that the contact area, A_r, includes both the total contact area of the pad asperities in direct contact with the wafer surface, A_{pw_total}, and the abrasives/wafer contact, A_{aw_total}. In other words, A_r is given by:

$$A_r = A_{pw\_total} + A_{aw\_total} \tag{14}$$

3.3.2. Contact force and contact area of single effective abrasive particle

During the CMP process, the abrasives embedded in the real contact area of the polishing interface penetrate into both the polishing pad asperities and the wafer surface causing the wafer surface to deform plastically.

As shown in Figure 9, the bulk of the abrasive particle becomes embedded in the polishing pad asperity surface rather than within the wafer surface. From Figure 9, it is clear that:

$$D = \delta_{ap} + \delta_{aw} \tag{15}$$

where x is the abrasive particle diameter, δ_a and δ_{aw} are the penetration depth of abrasive/pad contact interface and the penetration depth of abrasive/wafer contact interface, respectively.

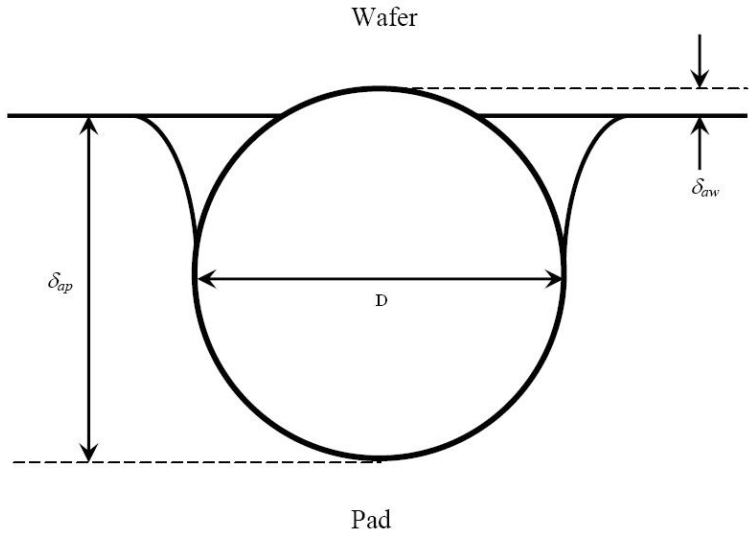

Figure 9. Schematic view of abrasive particles trapped at top of polishing pad

The present study assumes that the pad/abrasive contact interface undergoes elastic deformation and the wafer/abrasive contact interface is assumed to deform plastically. Zhao [47] indicated that the elastic contact force between the pad asperity surface and the abrasive particles can be described as:

$$F_{ap} = \frac{4}{3} \cdot E_{ap} \cdot \left(\frac{D}{2} \right)^{0.5} \cdot \delta_{ap}^{1.5} \tag{16}$$

where F_{ap} and E_{ap} are the contact force of the pad asperity and the abrasive contact and the equivalent Young's modulus of polishing pad and abrasive, respectively.

Furthermore, the plastic contact force of the particle and wafer surface contact is given by:

$$F_{aw} = H_w \cdot \pi \cdot D \cdot \delta_{aw} \tag{17}$$

where F_{aw} is the contact force for a single effective abrasive at the wafer/pad asperity contact and H_w is the hardness of the wafer surface.

Consequently, the force equilibrium on a single particle can be expressed as:

$$F_{abrasive} = F_{ap} = F_{aw} \tag{18}$$

Therefore, it can be shown that:

$$\frac{4}{3} \cdot E_{ap} \cdot \left(\frac{x}{2}\right)^{0.5} \cdot \delta_{ap}^{1.5} = H_w \cdot \pi \cdot D \cdot \delta_{aw} \tag{19}$$

Substitution of Equation (15) into Equation (19) enables the penetration depth of the wafer/abrasive interface to be solved from [47]:

$$\delta_{aw} + \left(\frac{9}{8} \cdot \pi \cdot \frac{H_w^2}{E_{ap}^2} - 3\right) \cdot D \cdot \delta_{aw}^2 + 3 \cdot D^2 \cdot \delta_{aw} - D^3 = 0 \tag{20}$$

The contact area and the contact force for a single effective abrasive particle at the wafer/pad asperity interface can be determined respectively from:

$$A_{aw} = \pi \cdot D \cdot \delta_{aw} \tag{21}$$

$$\begin{aligned} F_{aw} &= A_{aw} \cdot H_w \\ &= \pi \cdot D \cdot \delta_{aw} \cdot H_w \end{aligned} \tag{22}$$

where A_{aw} is the contact area for a single effective abrasive of the abrasives/wafer contact and F_{aw} is the contact force for a single effective abrasive at the wafer/pad asperity contact.

3.4. Results and discussion

3.4.1 Friction force analyses during polishing

It is assumed that an abrasive particle is pushed into a wafer surface through plastic deformation of the latter. Figure 10 shows the schematic drawing of the embedded particle on the wafer surface. Given the particle size we can assume the penetration depth is three times of the root mean square of the wafer surface asperities height ($3 \cdot \sigma_{asperity}$). By using the equation (21) and (22) derived from the modeling section, we can calculate the particle-wafer contact area and contact force for different particle size, as well as other parameters in order to find the friction force that removes the particle.

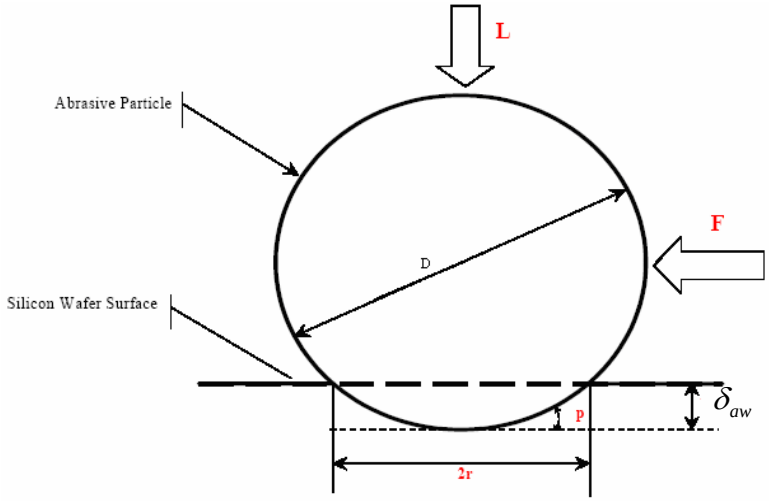

Figure 10. Schematic of the embedded particle on the wafer surface

Friction force is defined as [48]:

$$F = \pi r^2 s + r^2 \tan p \cdot m \qquad (23)$$

where s is the shear strength, m is the hardness of particle, and p is the surface roughness angle (as shown in Figure 10). The results of these calculations are tabulated in Table 1.

Figure 11(a) shows that under the same load, the different penetration depth can be achieved with different particle size. As seen in this figure, the penetration depth to the wafer surface increases linearly with the particle size. This is due to the available volume of the particle penetrates into wafer surface. It is assumed that the hardness of a particle is larger than that of the wafer.

Table 1. Friction force calculation

Particle Size (m) x	Penetration Depth (m) δ_{aw}	Particle-Wafer Contact Area (m^2)	Particle-Wafer Contact Force (N) L	Radius of Penetration (m) r_p	Angle (degree) p	Friction Force (N) F
5.0E-08	1.3682585789E-10	2.1492555501E-17	2.5791066602E-07	2.6155865297E-09	2.9945118610	4.2945584495E-09
1.0E-07	2.7365171578E-10	8.5970222006E-17	1.0316426641E-06	5.2311730595E-09	2.9945118610	1.7178233798E-08
1.5E-07	4.1047757367E-10	1.9343299951E-16	2.3211959942E-06	7.8467595892E-09	2.9945118610	3.8651026045E-08
2.0E-07	5.4730343157E-10	3.4388088802E-16	4.1265706563E-06	1.0462346119E-08	2.9945118610	6.8712935191E-08
2.5E-07	6.8412928946E-10	5.3731388754E-16	6.4477666504E-06	1.3077932649E-08	2.9945118610	1.0736396124E-07

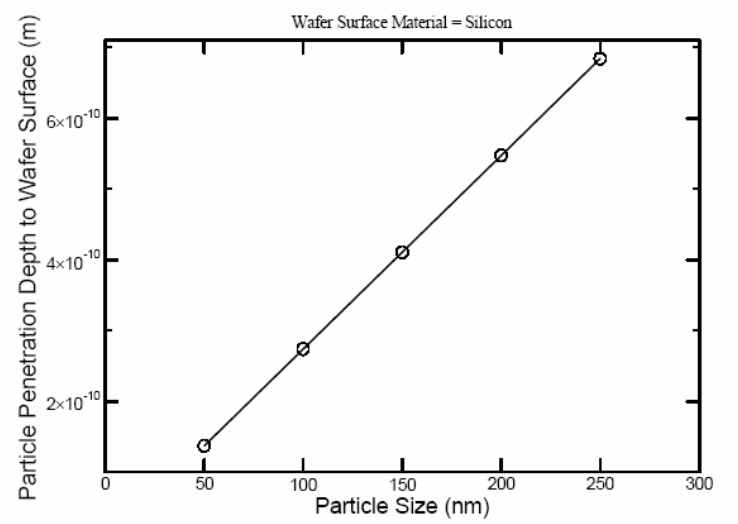

Figure 11(a). Different penetration depth can be achieved with different particle size

Figure 11(b) shows the resulting particle friction force due to different particle size. This friction force is the maximum tangential force an adhered particle stands

against. A higher tangential force would result the removal of the particle. On the other hand, under a certain tangential force, there is a maximum size of particles that are adhered to the wafer surface. Under a certain friction, larger (than the maximum size) particles can not be mechanically attached to a wafer surface. The smaller a particle is, the easier it is for it to be mechanically attached to the wafer surface.

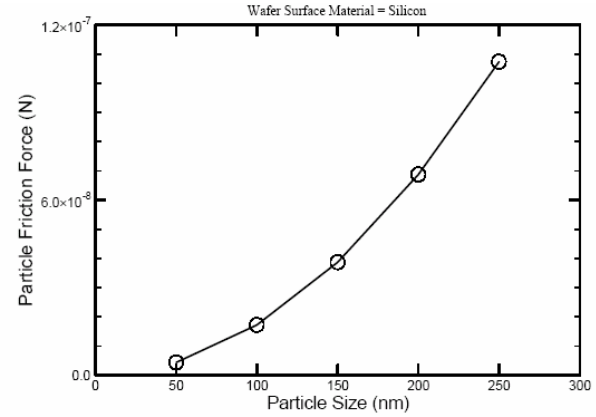

Figure 11(b). Resulting particle friction due to different particle size

3.4.2. Cleaning results

In previous sessions we discussed that during CMP, small particles are easier to be attached to a wafer surface. Here the cleaning of these attached particles is discussed. Silicon wafer surfaces were cleaned with water and with the surfactant. After cleaning experiments, surface analysis was carried out by using an Atomic Force Microscope (AFM). Figure 12 shows the remaining particles on the silicon wafer surface after the post-CMP cleaning process. In 412 μm^2 scan area, the average particle size of 4.38 μm and the average roughness value of 10.67 nm were obtained. These remaining particles were identified as individual or agglomerated silica particles by energy dispersive x-ray spectroscope (EDS). This adherence can be due to the asperity difference on the wafer surface and the higher attractive force in the interface during the polishing process, thus making the slurry particles cling to the wafer surface. The agglomerated particles have

been reported in the past [49]. It was found that particles tend to form agglomerate in the slurry solution at pH 7 or higher. Thus effective cleaning of these particles will require a combined interaction between the mechanical effort from the brush sweeping and the chemistry of cleaning solution (tribochemical interaction). As seen in Figure 12, the cleaning process was not effective since it only depends on the mechanical effort from the brush sweeping.

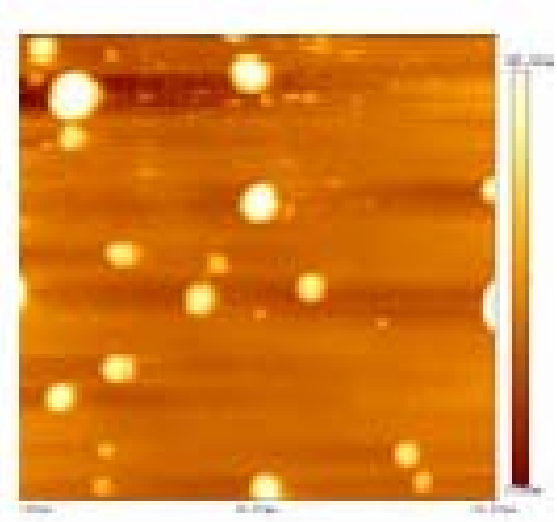

Figure 12. AFM image of cleaned wafer surface with deionized water. The scanned area is 412 μm^2

In order to see the combined effort of tribochemical interaction in the post-CMP cleaning, the sample from Figure 12 is cleaned again with a 0.1 %wt of AES anionic surfactant. Figure 13 shows the breakage of small particles within a big cluster due to the addition of surfactant. When surfactant is mixed with deionized water, the molecules will dissolve and form a layer of saturation on the surface. The bond strength of substrates is weakened and will in turn reduce the surface tension and thus allow the bond breaking of particle during brush sweeping motion. Moreover, the remaining surfactant molecules in the cleaning solution can stabilize the charge of the removed particles by attaching themselves to these particles and further, can create a repulsion zone between the wafer/particle and particle/particle as they come into contact in order

to prevent further adherence of these particles to the surface. Detailed discussions on surfactant molecules will be discussed in Chapter 4. The evidence is seen in Figure 13. The small particles were originally aggregated together through van der Waals force. This force is weakened due to lower surface tension thus reducing the average cluster size of clustered particles from 4.38 to 3.062 μm. The average surface roughness is further reduced to 6.41 nm. In the case of larger particles present in this figure, more mechanical force should be applied for complete particle removal. Additionally, soaking the wafer in the cleaning solution prior to the cleaning process will allow the surfactant to disperse homogeneously in the solution and thus, provide the synergistic mechanisms as described above.

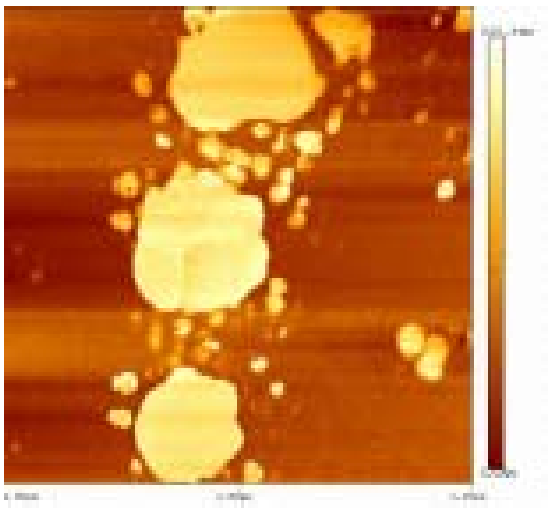

Figure 13. AFM image of cleaned surface with surfactant. The scan area is12 μm^2

The experimental results are further analyzed using the continuous mechanics method. The result is shown in Figure 14. As inferred from this figure, the force needed to remove particles change with particle size. After a certain size, the effectiveness of the mechanical removal is significantly reduced. After this stage, using surfactant will aid in reducing the force needed to remove a smaller particle.

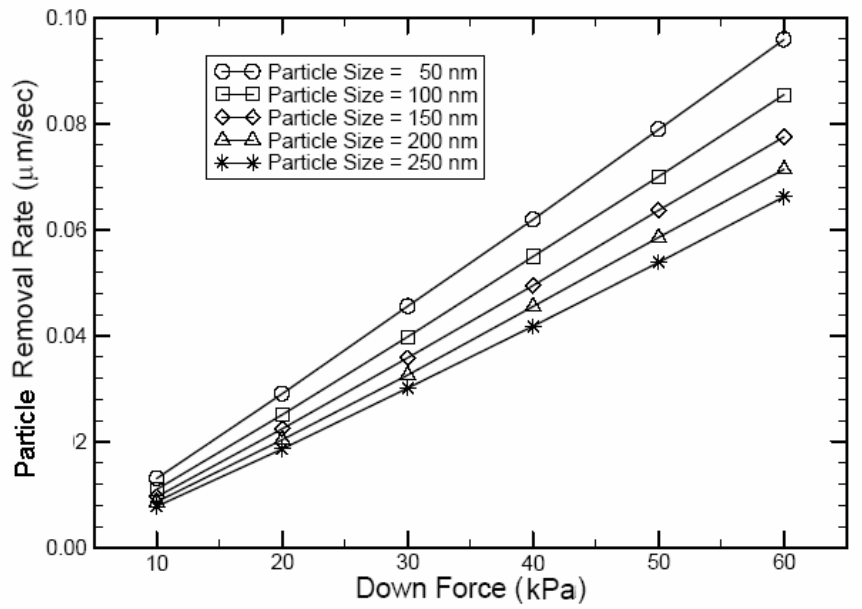

Figure 14. Variation of down force for different particle size

Furthermore, the addition of surfactant will also increase the cleaning solution pH. In order to validate this concept, five samples were cleaned without surfactant and another five samples with surfactant. The average results of these samples are tabulated in Table 2. At a cleaning solution pH of 8.36, the number of particles and the average particle size remaining on the surface is decreased as compared to the result without surfactant.

Table 2. A comparison result between post-CMP cleaning with and without surfactant

	Post-CMP without surfactant	Post-CMP with surfactant
Average particle size (μm)	9.85	6.02
No. of particles per area density	9.15	0.34
Cleaning solution pH	7.59	8.36

3.4.3. Adhesion force and energy required to remove one particle

In order to study the adhesion force in post-CMP cleaning, we will only consider the van der Waals force present on the interface between the particle and the wafer surface.

For an ideal case of a spherical particle adhesion in the wafer surface, we can use the following equation to estimate the van der Waals force [50], which can be expressed as:

$$F = \frac{A \cdot R}{6 \cdot r^2} \tag{24}$$

where A is the Hamaker constant, R is the radius of the particle, and d is the separation distance between the particle/substrate. In this study, the Hamaker constant of 7 eV and a separation distance of 3.68 Å will be used.

For post-CMP cleaning without surfactant, the adhesion force ranges from 1.15×10^{-5} to 4.54×10^{-6} N, and when surfactant is used, the force is greatly reduced from 7.03×10^{-6} to 0 N (calculated through the change of remaining particle radius after cleaning). From this calculation, we can estimate the amount of energy required to remove one particle during cleaning. The estimated energy is 4.60×10^{-15} J. With addition of surfactant, it becomes 2.81×10^{-15} J. It is seen that the addition of surfactant in the cleaning process proved to be effective in reducing the amount of energy (about 39% reduction) required to remove one particle.

3.4.4. Removal mechanisms during post-CMP cleaning

When the brush comes in contact with the particle, it will be compressed and loosen the van der Waals force between the particle and wafer surface. This force can be further loosened since the brush is moving reciprocally in a sweeping motion. During this process particles may be trapped to the brush pores due to the mechanical action of the brush sweeping or chemically absorbed on the brush. Nevertheless, the successful cleaning process will depend on the combined effort of the tribochemical interaction. Factors that might influence the cleaning process are the brush velocity, concentration of

surfactant, brush size and its pore structure, brush cycle and the size of adhered particle on the wafer surface.

3.4.5. Friction analyses in post-CMP cleaning

Experiments in this research showed that the average friction coefficient measured during the post-CMP cleaning process was around 0.7 (Figure 15). However, when the surfactant was added, this value is reduced to 0.2. It is clearly shown that with the addition of surfactant, the effectiveness of the cleaning is not in the reduction of friction force. Instead, it is due to the chemical nature of the particle removal. There are two effects for adding surfactant. One is to weakening the bonds between particles as shown in Figure 12. The other is for further prevention of the adherence of particles back to the wafer surface due to its repulsive barrier in the solid-liquid interface. This repulsive barrier is effective in reducing the number of particle count on the surface. As a result, a low friction was achieved.

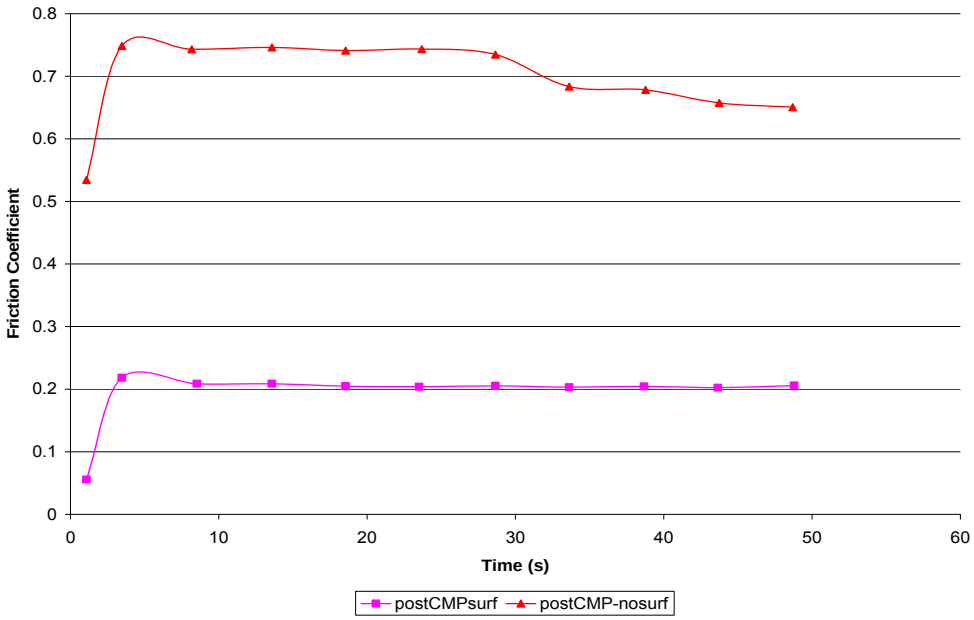

Figure 15. Friction coefficient vs. cleaning time during post-CMP cleaning

Furthermore, low friction is preferable in the cleaning process since it will prevent scratching. Low friction will also reduce further penetration of adhered particles on the wafer surface during the cleaning process which gives higher cleaning rate by the brush sweeping.

3.5. Conclusions

In this research we investigated the particle adhesion and removal mechanisms during CMP and post-CMP cleaning using experiments combined with numerical analysis.

Results showed that mechanical removal is only effective for a certain sized large particles. Once the particle size reaches a critical size, the remaining small particles will not be removed effectively. For remaining small particles, adding surfactant can effectively removal particles. The surfactant has two basic effects. One is to weaken the bonds between particles and particles and surfaces. The other is to prevent further adhesion between particles and wafer surface.

This research opens areas of future investigation in understanding roles of surfactant molecules in the post-CMP cleaning. In this regard, we will observe how the surfactant behavior before and after it reaches the critical micelles concentration (CMC). The tribological approach over a range of surfactant concentration and temperature will be discussed.

CHAPTER IV

ROLE OF SURFACTANT MOLECULES DURING POST-CMP CLEANING

4.1. Introduction

Post-CMP cleaning used to be a simple process of rinsing with deionized water to remove slurry particles. However, they must now incorporate additional chemistries or additives for effective particle removal. The recent development of effective post-CMP cleaning solutions is useful in achieving the reduction in rinse water consumption. Thus the usage of surfactant along the deionized water will help in reducing consumable cost. Particle removal is of utmost importance and any post-CMP cleaning chemistry used will have to overcome or modify the surface charge of the wafer and surface charge of particles. The electrostatic surface charges may vary as a function of particle size and ionic strength which might lead to complications during cleaning. In addition to that, temperature of the rinse solutions and also non-charged particle adhesion may demand special post-CMP cleaning chemistries.

The complexity of the cleaning process is partly due to the unique structure of a surfactant. When a long-chained organic head group comes into contact with a particle, it will reduce the bond strength of the particle as it react with particles and encircles the particles as shown in Figure 16. However, in order to easily repel the particle, a lesser amount of the non-dominant surface charge has to be present. This will increase the zeta potential or repulsive charge between particle and substrate. Also if surface tension is reduced, the van der Waals (vdW) force present in the system will be weakened, thus increasing particle removal during brush sweeping.

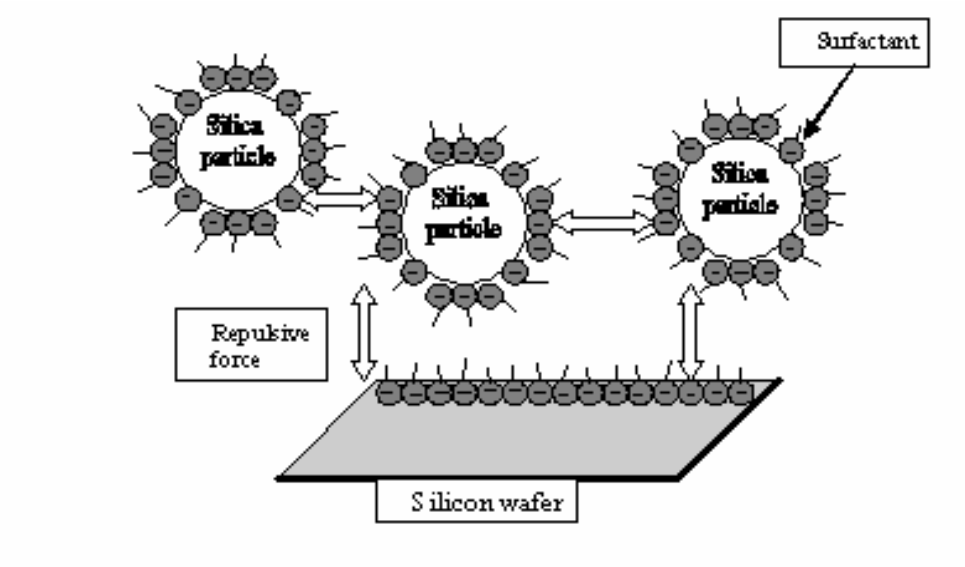

Figure 16. Schematic representation of repulsive barrier due to the formation micelles in the solid-liquid interface

Since particle contamination on the surface may damage the subsurface on the layer of interconnect, tremendous efforts have been focus in the particles removal. Two cleaning methods have been proposed, one being direct contact cleaning which employed double sided brush and non contact cleaning which only use chemical solution.

Because direct contact cleaning is proven more effective in particles removal [33,43,45,51], numerous study has been done to understand the cleaning process. These studies consist of proposing the adhesion model to investigate the particle removal mechanism [36,42,52,53]. Further work has been focus on the hydrodynamics effect [6,33,34,43], analyzing the brush effects and the cleaning speed [34,35,54,55], modifying the solution pH [45,56] to control the electrostatic forces, and even introducing the surface-active agents or surfactants in the cleaning solution to improve the cleaning efficiency [57-59].

An example of surfactant in cleaning solution is as follows, Liu et al. used a surfactant to clean the polished silicon wafer in conjunction with a chelant to remove metallic contamination [58]. Results showed that these chemicals were effective in

prevent surface contamination. However, the details of how the surfactant promotes cleaner surface was not well-understood. Similarly, among many other articles published on using surfactants, the types and concentration of surfactants were not stated [57-60].

The objective of this study is to investigate the effects of surfactants and mechanisms in post-CMP cleaning. In order to understand roles of surfactant molecules on post-CMP cleaning, for the first time, we use a tribological approach over a range of surfactant concentration and temperature. In this regard, we observe how the surfactant behavior before and after it reaches the critical micelles concentration (CMC). Based on our study, we propose an interactive explanation of surface molecules with the wafer surface and nanoparticles through friction. This understanding will serve as a guide on using surfactant in order to achieve effective particle removal.

4.2 Experiments

Nine 1.6 cm x 1.6 cm silicon wafers were prepared for the cleaning experiments. These samples were previously polished with silica slurry at room temperature. The applied pressure used was 17 kPa and the polishing platen rotated at a constant speed of 10 cm/s for 30 minutes.

The cleaning experiments were performed on a disk-on-disk tribometer (CSM). The brush was used as the upper disk and the wafer was the lower one. The polyvinyl alcohol (PVA) brush (Rippey) was used for this study. Nine cleaning solutions were made by mixing 10 mL deionized water with 0.1, 0.2, 0.3, 0.4, 0.5, 0.6, 0.7, and 1 wt % anionic surfactant containing alcohol ether sulfates (AES), respectively. Prior to data acquisition, the brush, 5 mm in diameter, was soaked in deionized water for 30 minutes. The cleaning experiment was performed at room temperature with the following parameter: the brush pressure was 125 Pa and the speed was 0.5 cm/s. The brush moved in a reciprocating at three locations across the wafer. Following the cleaning process, the sample was cleaned with deionized water in an ultrasonic cleaner for 1 minute to prevent redeposition of particles to the substrate.

In order to see the roles of surfactant molecules (micelles) in post-CMP Cleaning, further experiments were carried out by using small angle x-ray scattering

spectroscope (SAXS) as shown in Figure 17. With SAXS the micelles formation can be characterized in terms of its size, distribution and dispersion in the liquid solution. As for sample preparation, five cleaning solutions contain different surfactant concentration (0.3, 0.75, 1, 1.5, 2 %wt, respectively) are mixed with water and a few drop of silica nanoparticles. The reason we add the silica particles here is to see the monolayer or bilayer formation of micelles as it reacts with the silica particles. The operating parameters for the experiments are as follows: operating time is 24000 second, the volume of solution is 2 mL, and operating temperature is 25^0C.

Figure 17. Small angle x-ray scattering spectroscopy (SAXS)

4.3. Results and discussion

4.3.1 Friction analyses in post-CMP cleaning

Figure 18 and 19 show effects of concentration of surfactant and temperature as a function of friction coefficient during post-CMP cleaning. Results show that as we increase the concentration of surfactant and temperature, the average friction coefficient is reduced. This phenomenon can be explained as the following. Since at high

temperature, the surfactant will take less time, than at low temperature, to disperse homogeneously to the substrate surface which in turns reduces the surface tension. Lower surface tension will give lower wetting angle. Moreover, lower wetting angle creates higher wetting, thereby reducing the average friction coefficient on the substrate surface. In such situations, the process promotes particle removal during brush sweeping. Another reason is that the silicon wafer is prone to exothermic reaction during the cleaning process; hence an increase in temperature at the interface will reduce the average friction coefficient of the substrate surface. Furthermore, as discussed earlier, low friction is preferable in the cleaning process since it will prevent scratching. Low friction will also reduce further penetration of adhered particles on the wafer surface during the cleaning process which gives higher cleaning rate by the brush sweeping.

As shown in Figure 18, the friction coefficient will eventually reduce to minimum if the surfactant molecules completely wet the surface**.** Further analyses on this behavior will be provided in the next section.

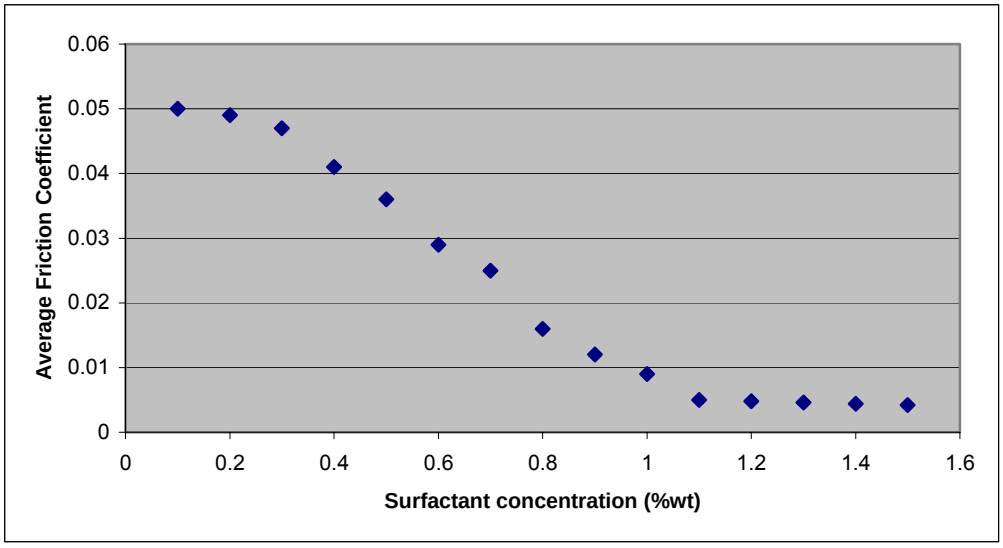

Figure 18. Surfactant concentration (%wt) as a function of average friction coefficient

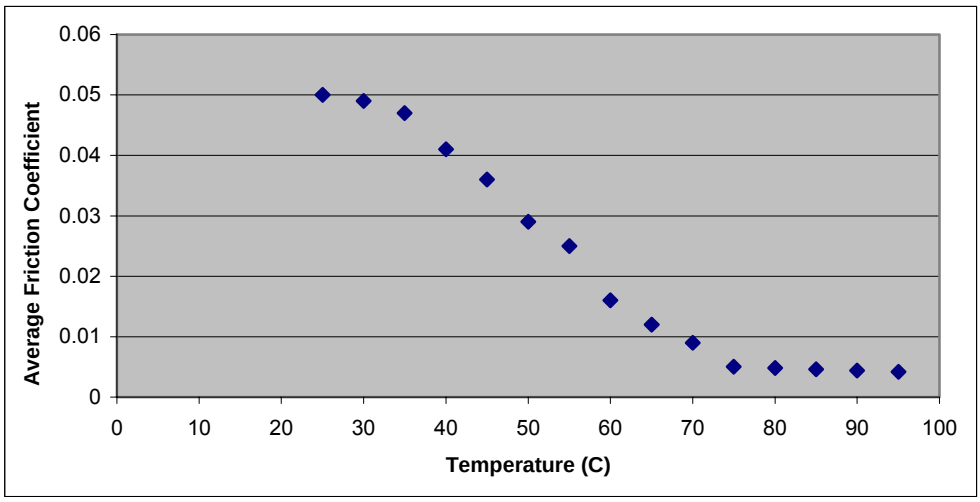

Figure 19. Temperature (^{0}C) as a function of average friction coefficient

4.3.2. Micelles formation in cleaning solution

The effect of surfactant is further analyzed with a small angle x-ray scattering spectroscope (SAXS). Figure 20 shows the scanning intensity of micelles formation of different surfactant concentration mixed with deionized water and a few drop of silica nanoparticles as a function of scattering factor (s). As shown in figure 20, the micelles formation is the highest at concentration 1%wt with a mean radius gyration of 5.70 nm. At this point the surfactant will have the highest amount of micelles to wet the substrate; the higher wetting on the surface will reduce further the friction coefficient thus provide better cleaning result as shown in Figure 18.

Figure 20 shows that at concentration of higher than 1 %wt, the micelles formation begins to drop at 1.5 %wt and further reduced at 2 %wt. This result indicates that cleaning should be performed at concentration less than 2 %wt. At concentration of 2 %wt, the cleaning will not be effective due to less micelles formation in the cleaning solution as it will be too concentrated. Less micelles and foaming in the cleaning solution will not be useful in the cleaning application.

From the SAXS it was shown that the micelles at different concentrations have a spherical shape. Figure 21 shows the example of this spherical micelle at 1 %wt with the mean radius gyration of 5.70 nm.

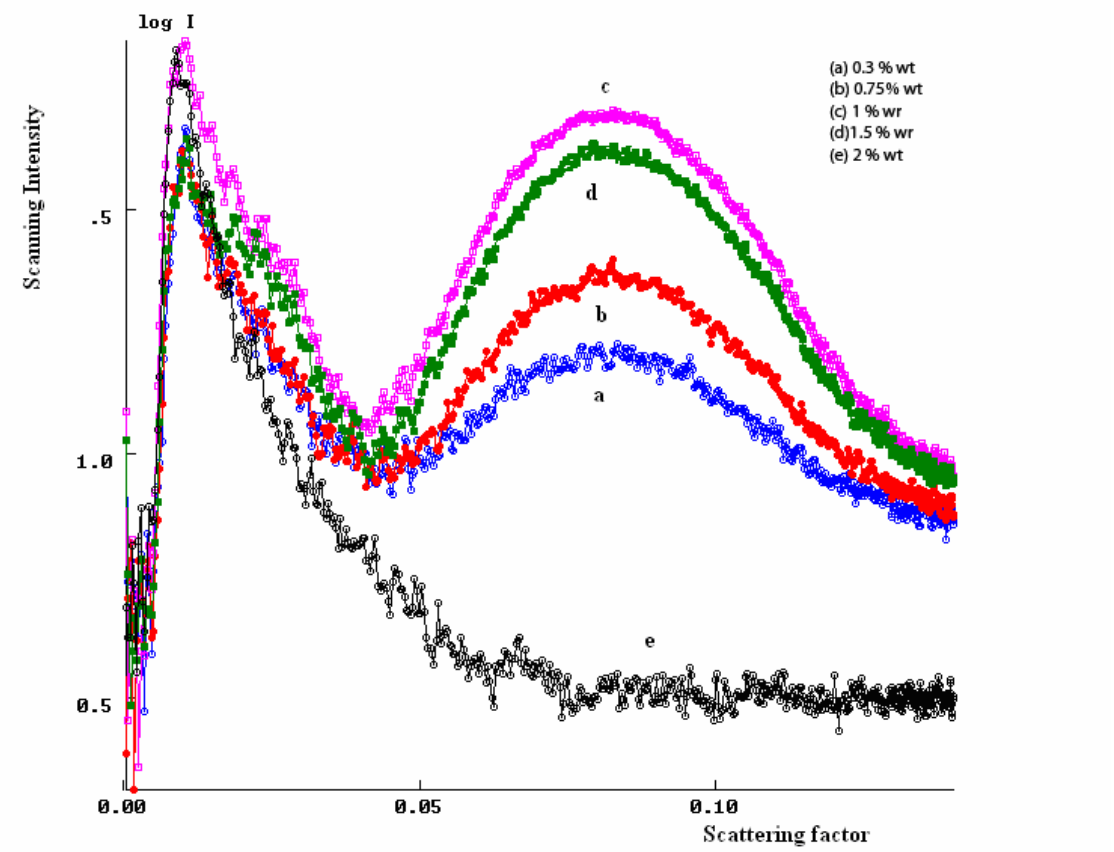

Figure 20. The scanning intensity of micelles formation as a function of scattering factor

To calculate the radius of the actual micelle we need to use the following equation:

$$R_m = \sqrt{\tfrac{5}{3}} \cdot Rg \qquad (25)$$

where R_m is the actual radius and Rg is the radius of gyration.

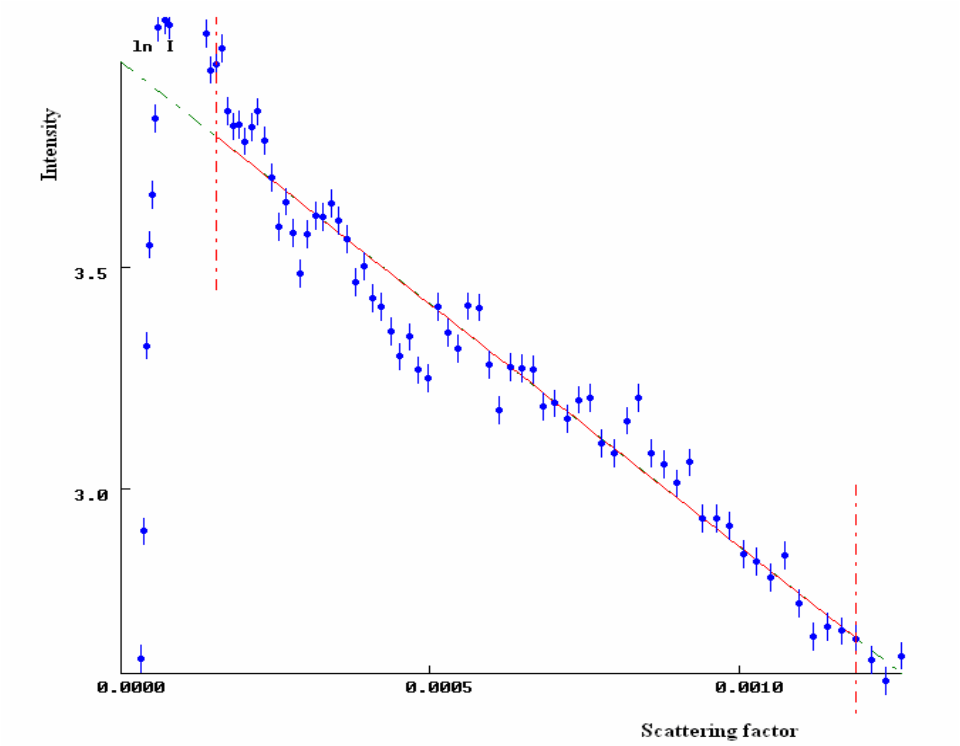

Figure 21. The mean radius gyration for 1 %wt concentration

Thus the mean actual radius of the micelle at 1 %wt is 7.359 nm. Table 3 shows the mean actual radius for each surfactant concentration. As seen in Table 3, the mean actual radius for 0.75 %wt is the same as that for 1 %wt. However the numbers of micelles present in 1 %wt are higher due to the high concentration of surfactant in the cleaning solution. As can be seen in Table 3, the mean radius of gyration increases from 0.3 to 0.75 %wt, reach maximum from 0.75 to 1%, and drop is significant at 2 %wt. The change in radius is expected since the solution become too concentrated.

Table 3. Mean actual radius of micelle for each surfactant concentration

Surfactant concentration (%wt)	0.3	0.75	1	1.5	2
Radius of gyration (nm)	5.24	5.7	5.7	4.9	4.5
Actual radius (nm)	6.765	7.359	7.359	6.326	5.809

4.3.3. Surface tension of the clean surface

In order to see the effectiveness of cleaning with different surfactant concentration, we evaluate the cleanliness of the wafer surface by measuring the contact angle (Figure 22). To do so, we use the syringe to deliver one droplet of deionized water to the cleaned surface. Results are tabulated in Table 4.

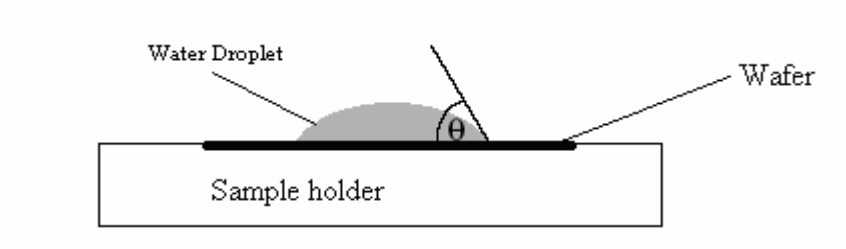

Figure 22. Schematic diagram of a contact angle, θ measurement

Table 4. Contact angle measurement for the clean surface

Surfactant concentration (%wt) used in cleaning	0.1	0.2	0.3	0.4	0.5	1
Contact angle (^{0})	71	54	49	43	41	21
Surface tension (mN/m)	92.1	51	45.7	41	39.7	32.3

As inferred from Table 4, cleaning with 1%wt surfactant gives the smallest contact angle, whereas cleaning with 0.1 %wt surfactant concentration results in highest contact angle. Smallest contact angle means good wetting and cleaning surface, whereas a high contact angle exhibits poor cleaning surface. This phenomenon can be explained by the change in surfactant concentration which leads to a change in surfactant adsorption. An increase in the surfactant concentration produces an outcome of a decrease in the contact angle, which indicates the surface hydrophilicity. This decrease in the contact angle is attributed to the adsorption of surfactant at the wafer surface. Small contact angle also means lower surface tension, with the addition of surfactant

concentration from 0.1 to 1 %wt the surface tension is reduce from 92.1 to 32.3 mN/m. This indicates that smaller surface tension was due to higher wetting on the cleaned surface; thereby reduce the friction coefficient significantly.

4.3.4. Surface topography of clean surface

For post-CMP cleaning brush-particle must come into contact for complete particle removal. For small particles, brush sweeping with surfactant proved to be effective. In the case of larger particles as shown in Figure 23, higher concentration of surfactant and higher operating temperature are proved to be effective in reducing the size of residual particles adhere to the substrate surface.

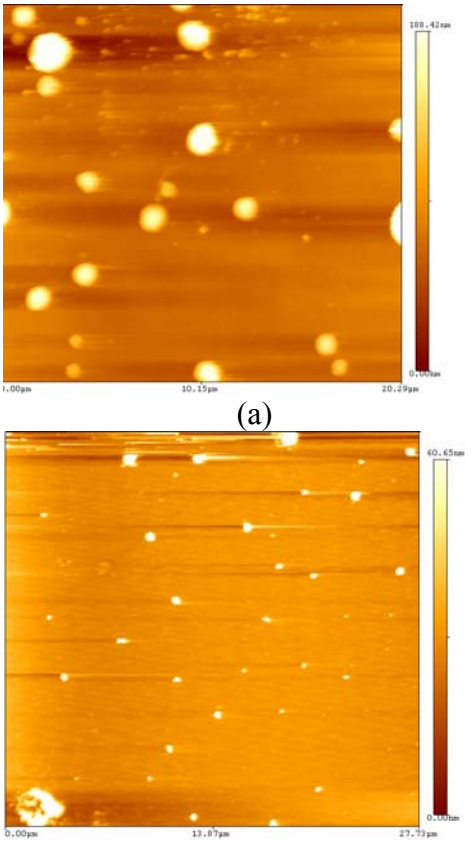

(a)

(b)

Figure 23. AFM image of silicon surface after post-CMP cleaning with different amounts of surfactant (a) at 0.1 %wt surfactant, (b) at 0.7 %wt surfactant

4.4. Conclusions

In this research we used a new approach to investigate the particle removal mechanisms during post-CMP cleaning. The approach starts with polishing experiments in order to adhere particles on the wafer surface. The chemical environment is specifically designed for this purpose. After polishing, cleaning experiments are conducted to study particle removal mechanisms. The selection of surfactants was as well specifically considered. Results showed that surfactant molecules can reduce the adhesion between particles. For larger particles, cleaning with higher concentration of surfactant and higher operating temperature proved to be effective in reducing the size of residual particles adhered to the substrate surface. The mechanisms were dominated by interfacial interactions.

CHAPTER V

MODELING OF ADHESIVE FORCES ON ELASTIC SURFACES-AN ELASTICITY THEORY APPROACH

5.1. Introduction

Interfacial forces are important factors obtaining effective post-CMP cleaning. During CMP, particles can adhere to the wafer surface due to surface interactions [53]. The surface charge between the particle and substrate surface also promotes electrostatic attraction [61]. Moreover, during polishing, particles might deform since they were pressed against the wafer surface and the polishing pad. In this study, an elasticity method is applied to understand the post-CMP mechanisms. The advantages of using elasticity theory are several. Firstly, it is desirable to eliminate plastic deformation and scratches during cleaning. Therefore, elasticity approach is more favorable. Next, the elasticity theory is useful in studying the contact between real engineering surfaces. Real engineering surface is not perfectly free from irregularities as it contains peaks and valleys with predominant surface features transmitted by the last finishing process. Thus even in the presence of lubricant, it is a normal circumstance for the asperities of two such surfaces to interact when run against one another under a load. Although the subject of surface interactions has received considerable attention, the effect of real loading and real material behavior have not been sufficiently explored. This study can best be achieved by an asperity-based approach.

It has been observed that abrasive particles do not always retain their original shape due to deformation [62]. It is therefore reasonable to assume a cylindrical shaped particle for simplicity in our analyses.

In order to study the effect of van der Waals force on surface deflection, it is assumed that the irregular particle is rigid. The resulting deformation of the elastic surface can be obtained using the theory of elasticity as shown in Figure 24 (a) and (b).

This is due to the fact that the deformations will be small as compared to the dimensions of the particle.

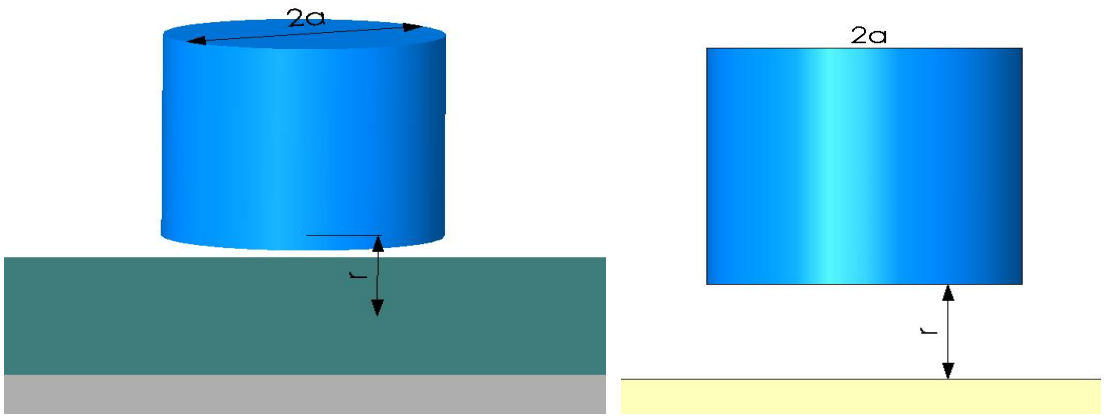

Figure 24 (a). No surface deformation

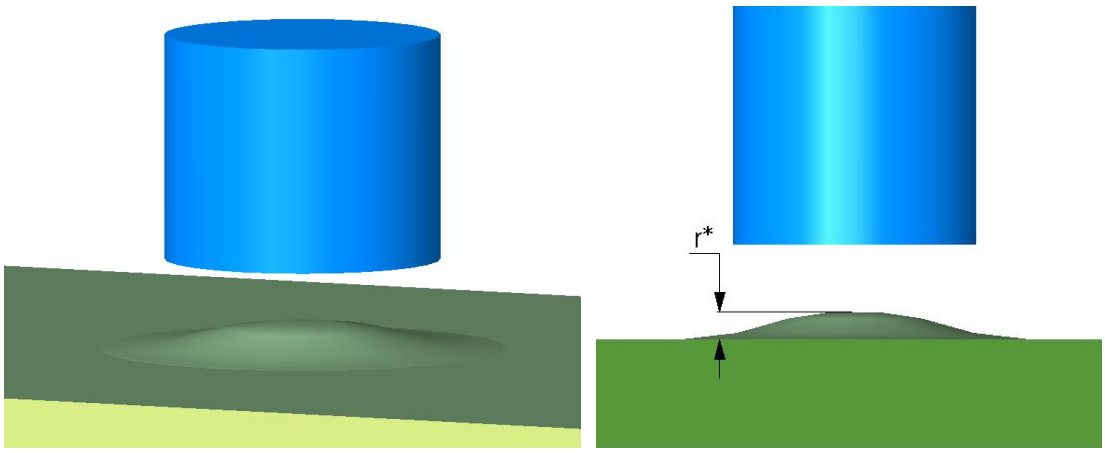

Figure 24 (b). Surface deformation

The problem under consideration here involves a rigid cylindrical shaped particle and an elastic surface. This problem will be approached by using plane stress assumptions [63,64]. Moreover, the analysis involves a case where the driving forces are the van der Waals forces of attraction and repulsion. This research focuses on the investigation of the deflection of surface due to the van der Waals force.

In order to approach the problem by using the theory of elasticity, the following assumptions are made:

- As the distance between the surfaces is decreased, the van der Waals forces deform the elastic surface. It is assumed that the deformation of each point of the elastic surface is the same. However, in reality, this deformation is not uniform at each point of the elastic surface. To avoid the nonuniformity problem, it is conveniently defined the deformation at the mid-point of the deflected surface and assumed this mid-point to be a true representative of each of the other points of the elastic surface.
- Only van der Waals forces are used in calculations since it is more dominant in interfacial adhesion thus the effect of electrostatic force is neglected to simplify the complexity of the problem under consideration.
- A semi-infinite plate is also assumed and neglected the effect of the other half plane.
- The problem for plane stress condition has already been solved.

5.2 Analysis

5.2.1. van der Waals force expression

To study the lift-up force of particle on the surface, it is imperative to understand the principle of attractive and repulsive forces on the surface. The strength at which these two forces balance is called Lennard-Jones potential. The Lennard-Jones potential contains a long-range van der Waals attraction and short range repulsion and is described by the following equation:

$$U(r) = 4\varepsilon\left[\left(\frac{\sigma}{r}\right)^{12} - \left(\frac{\sigma}{r}\right)^{6}\right] \tag{26}$$

where U is the Lennard-Jones potential in Joule, r is the separation distance in nm, σ and ε are the specific Lennard-Jones parameters, different for different interacting particles.

The variation of energy with the distance between the two particles is shown in Figure 25.

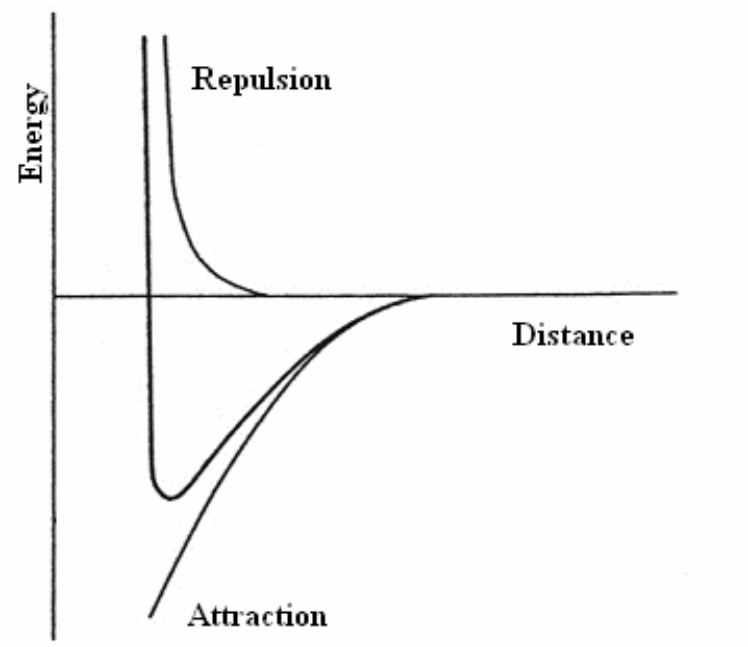

Figure 25. The Lennard-Jones potential

When the r is very small, the $1/r^{12}$ term dominates, and the potential is strongly positive. Hence the $1/r^{12}$ term describes the short range repulsive potential due to the distortion of the electron clouds at small separations. In contrast the $1/r^{6}$ predominates when the separation r increases in magnitude. Hence the $1/r^{6}$ term describes the long range attractive tail of the potential between two particles.

Furthermore, the equation above can be written as:

$$U = \left(\frac{B}{r}\right)^{12} - \left(\frac{C}{r}\right)^{6} \tag{27}$$

where $B=4\varepsilon\sigma^{12}$ and $C= 4\varepsilon\sigma^{6}$

The constant values of A and C can be obtained from the table 5 below.

Table 5. Lennard-Jones potential parameters [65].

Interaction	A (KJ/mol-nm^{12}	C (KJ/mol-nm^{6})
O-O	2.6331x10^{-6}	2.6171x10^{-6}
O-Cl	4.0635x10^{-5}	6.1404x10^{-5}
Si-O	3.0100x10^{-6}	3.2749x10^{-6}
Si-Cl	4.6474x10^{-5}	7.7658x10^{-5}
Cl-Cl	1.0691x10^{-4}	1.3804x10^{-4}

To find the force from the Lennard-Jones potential we can simply do the differentiation of U with respect to r, as follow:

$$F_{lj} = \frac{dU}{dr} = \frac{(-12)A}{r^{13}} - \frac{(-6)C}{r^{7}} \tag{28}$$

$$F_{lj} = \frac{-12A}{r^{13}} + \frac{6C}{r^{7}} \tag{29}$$

Using the maxima condition, it is determined that the maximum value of the force is obtained for r= 0.387722 units.

5.2.2. Expression for the deformation at the mid-point of a surface

5.2.2.1. Uniformly distributed vertical loading of a straight boundary

As previously mentioned, the van der Waals force acts as the driving force in this case. The elastic surface will deform due to the influence of this force. If this force exerts a uniform load of intensity “q” distributed over a portion of the boundary of a semi-infinite plate, the corresponding components of stress and hence, the stress field at

any point of a straight boundary under the influence of this vertical uniformly distributed load can be obtained by the use of a stress function. This function is called the Airy stress function and it satisfies the Bi-harmonic equation. The stress function is given by the relation:

$$\phi = Ar^2\theta \tag{30}$$

where A is a constant. The corresponding stress components for this stress function are:

$$\sigma_{rr} = \frac{1}{r}\frac{\partial \phi}{\partial r} + \frac{1}{r^2}\frac{\partial^2 \phi}{\partial \theta^2} = 2A\theta \tag{31}$$

$$\sigma_{\theta\theta} = \frac{\partial^2 \phi}{\partial r^2} = 2A\theta \tag{32}$$

$$\sigma_{r\theta} = -\frac{\partial}{\partial r}\left(\frac{1}{r}\frac{\partial \phi}{\partial \theta}\right) = -A \tag{33}$$

The above expressions for the stresses show that there acts a uniformly distributed shearing force of intensity (–A) and a uniformly distributed normal load of the intensity $A\pi$, abruptly changing sign at the origin.

From the stress relations, we can determine the components of the strain matrix in polar co-ordinates as follow. Let the components of the displacements in the radial and tangential directions be u and v.

Strain in the radial direction is given by the expression,

$$\varepsilon_{rr} = \frac{\partial u}{\partial r} \tag{34}$$

Also, from Hooke's law equation for radial strain for plane stress,

$$\varepsilon_{rr} = \frac{1}{E}(\sigma_{rr} - \nu\sigma_{\theta\theta}) \tag{35}$$

From the two relations above, we get

$$\frac{\partial u}{\partial r} = \frac{1}{E}(2A\theta)(1-\nu) \tag{36}$$

On integrating the above equation, we get the following expression for u.

$$u = \frac{2A}{E}(1-\nu)r\theta + f(\theta) \tag{37}$$

In the above expression, f(θ) is a function of θ only.

The strain in the tangential direction depends not only on the displacement "v" but also on the radial displacement "u". The total tangential strain is thus given by the expression,

$$\varepsilon_{\theta\theta} = \frac{u}{r} + (\frac{1}{r}\frac{\partial v}{\partial \theta}) \tag{38}$$

Also, from Hooke's law equation for tangential strain for plane stress,

$$\varepsilon = \frac{1}{E}(\sigma_{\theta\theta} - \nu\sigma_{rr}) \tag{39}$$

On equating the above expressions as shown below, we get an expression for v.

$$(\frac{2A\theta}{E}(1-\nu) + \frac{f(\theta)}{r}) + \frac{1}{r}\frac{\partial v}{\partial \theta} = \frac{2A\theta}{E}(1-\nu) \tag{40}$$

On simplification, it gives the following expression,

$$\begin{aligned} \frac{\partial v}{\partial \theta} &= -f(\theta) \\ v &= -\int f(\theta)d\theta + f_1(r) \end{aligned} \tag{41}$$

where $f_1(r)$ is a function of r alone.

Similarly, the shear strain is given by the following expressions:

$$\varepsilon_{r\theta} = \frac{\sigma_{r\theta}}{G} = -\frac{A}{G} \tag{42}$$

Also, from Hooke's law expression, we have

$$\varepsilon_{r\theta} = \frac{1}{r}\frac{\partial u}{\partial \theta} + \frac{\partial v}{\partial r} - \frac{v}{r} \tag{43}$$

Equating the two equations as shown below,

$$\begin{aligned} -\frac{A}{G} &= \frac{2A}{E}(1-\nu) + \frac{1}{r}\frac{\partial f}{\partial \theta} + \frac{1}{r}\int f(\theta)d(\theta) + \frac{\partial f_1}{\partial r} - \frac{1}{r}f_1(r) \\ &= \frac{1}{r}[\frac{2Ar}{E}(1-\nu) + \frac{\partial f}{\partial \theta}] + \frac{\partial f_1}{\partial r} + \frac{1}{r}\int f(\theta).d\theta - \frac{1}{r}f_1(r) \end{aligned} \tag{44}$$

On solving the partial differential equations separately, the solution will be of the form,

$$f(\theta) = 0 \qquad f_1(r) = -\frac{4A}{E} r \log(r) \tag{45}$$

Hence the displacement field obtained is of the following form:

$$u = \frac{2A\theta r}{E}(1-\nu) \qquad v = -\frac{4A}{E} r \log r \tag{46}$$

For the case of a semi-infinite plate,

$$A = \frac{q}{\pi} \tag{47}$$

5.2.2.2. Vertical displacement at the mid-point

The displacement at the center, the midpoint of the edge as shown in Figure 26 is given by,

Figure 26. Schematic drawing of vertical displacement of surface at the mid-point

$$v_a = -\frac{4}{E} * \frac{q}{\pi} * (a \log a)$$

$$= -\frac{2q}{\pi E}(2a \log a) \tag{48}$$

We have considered compressive forces while deriving this expression whereas in our problem, the forces on the elastic surface are tensile, hence the expression for deformation is

$$v_a = \frac{2q}{\pi E}(2a \log a) \tag{49}$$

which is used for further analysis.

5.2.2.3. Outline of the procedure

The following procedure is used in the analysis. The material of the surfaces considered in this work is silicon oxide. The corresponding values for A and C for this material have been chosen from the tabular column shown previously.

$A = 3.01 \times 10^{-6}$ KJ / mol-nm^2 $C = 3.2749 \times 10^{-3}$ KJ / mol-nm^6

5.2.2.4. Definition of ALPHA

To simplify the analysis, we define the non-dimensional parameter ALPHA as follow:

$$\text{ALPHA} = \left(\frac{r_i}{2a}\right) x10^9 \qquad (50)$$

where r_i is the distance between the particle and the elastic surface and a is radius of the particle

The input parameter is the distance between the particle and surface that is made dimensionless by assuming a ratio of the distance between two surfaces to the diameter of the particle. The input parameter, i.e., the ratio, is called ALPHA. The force acting between the surfaces is a known function of this parameter. For a given input of ALPHA, the force has been initially calculated. As a result, the effective distance between the surfaces decreases with the increase of initial force. The ALPHA value changes accordingly. Further more, for this new value of ALPHA, the force is recalculated. This again results in a change of ALPHA. This iterative procedure is continuously carried out till a stage where the force value which we calculated using our iterated ALPHA is almost the same as the one we calculate using the recalculated value of ALPHA.

5.2.2.5. Definition of error %

To determine the accuracy of the two values of the force calculated, we define an error in forces as shown:

$$\text{Error} = \left(\frac{F_{i+1} - F_i}{F_i} \right) x100 \qquad (51)$$

In this research, we have set the error percentage to be 0.0002%. We calculate ALPHA till error value reaches the desired value of error for any specified initial ALPHA. To find the trend of variation of van der Waals force for different values of ALPHA, we plot the values of initial force against the ALPHA. Figure 27 illustrates that the peak values of the initial forces are attained at a value of ALPHA close to and a little less than 80.

By interpreting Figure 27, we are able to surmise as to what range of values of ALPHA will result in domination of attractive forces over the repulsive forces.

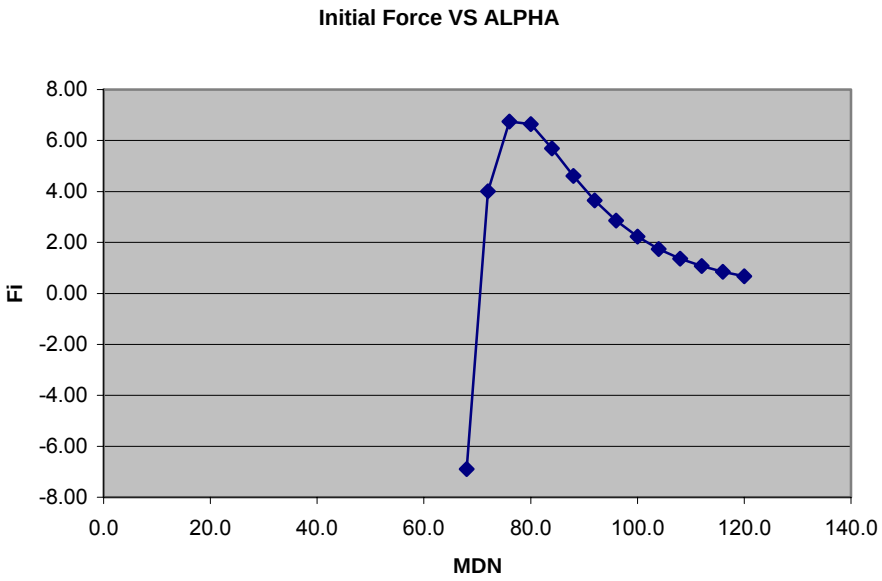

Figure 27. Initial force vs. ALPHA

Thus far we successfully reach upon the approximate value of ALPHA where the initial value of forces reached a peak. We chose a random value of 77.71 for ALPHA

and plotted Figure 28 of the error % against the ALPHA. We also tabulated the number of iterations required for the solution to converge by using a range of ALPHA values. We observed that the error % converged to the set value in the 14th iteration.

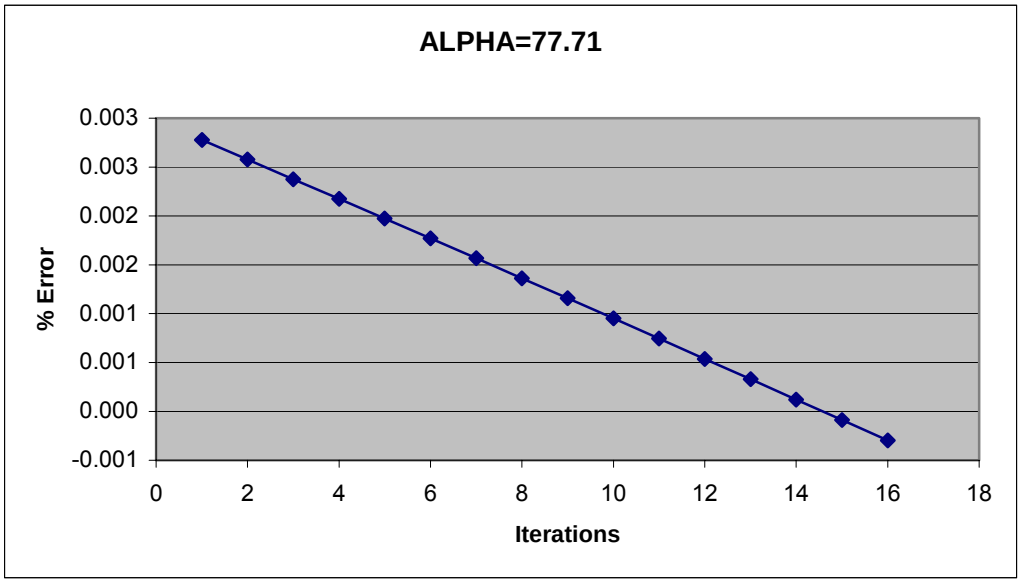

Figure 28. For an assumed ALPHA equal to 77.71

Figure 29 illustrates that for an initial value of 77.71 of ALPHA, the error value converges to the desired value for ALPHA's final value of 77.545.

Furthermore, initially, we note from the previous figures that when the distance between the surfaces decreases, the forces between the surfaces increase. This is misleading since it gives the general notion that the closer the surfaces, the larger the force. This is only true for certain conditions. As the distance between the particle and the surface is further decreased, attractive forces tend to reach a peak value after which repulsive forces tend to gain prominence over the attractive forces. As a result, two solid substances tend to repel each other. It is obvious that the peak values of the force between the surfaces reaches a peak value at a particular distance. In this research, we

outline the procedure to find out values for SiO_2 surface. This approach can extend to a broader application for any surfaces.

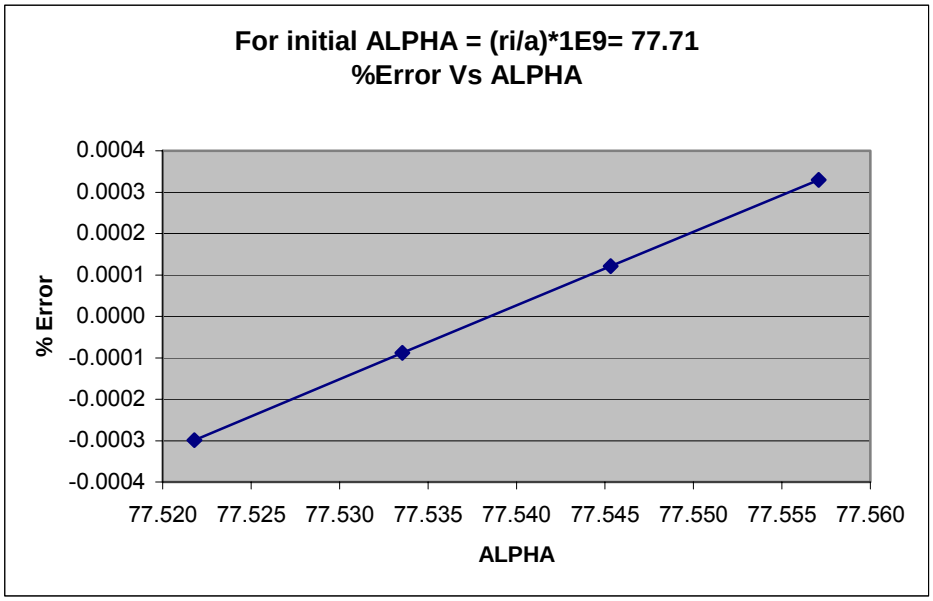

Figure 29. %Error vs. ALPHA for an initial ALPHA

5.3. Results and discussion

A trial-and-error approach was used initially with the ALPHA being 100. Figure 30 shows that the value of the error does not converge. In fact, the error increases with the number of iterations which is in contradiction to our objective. To improve, we reduced ALPHA value.

We next assigned a value of 90 to ALPHA. Figure 31 plotted shows that for this value of ALPHA, the error in forces converged to the required value. However, it took a whopping 1320 trials. To improve, we further reduced our ALPHA value.

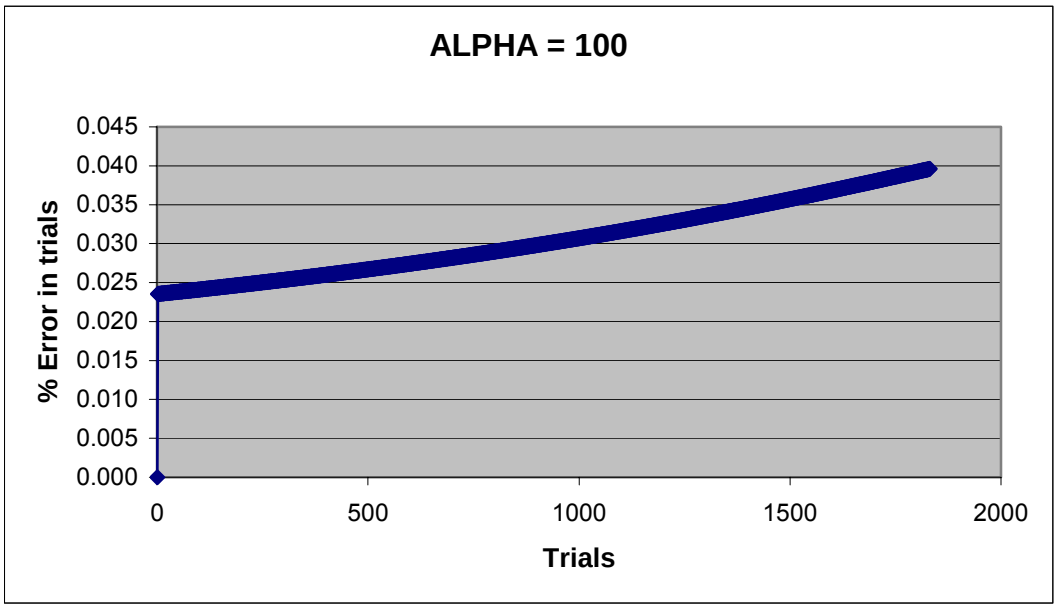

Figure 30. %Error vs. ALPHA for ALPHA =100

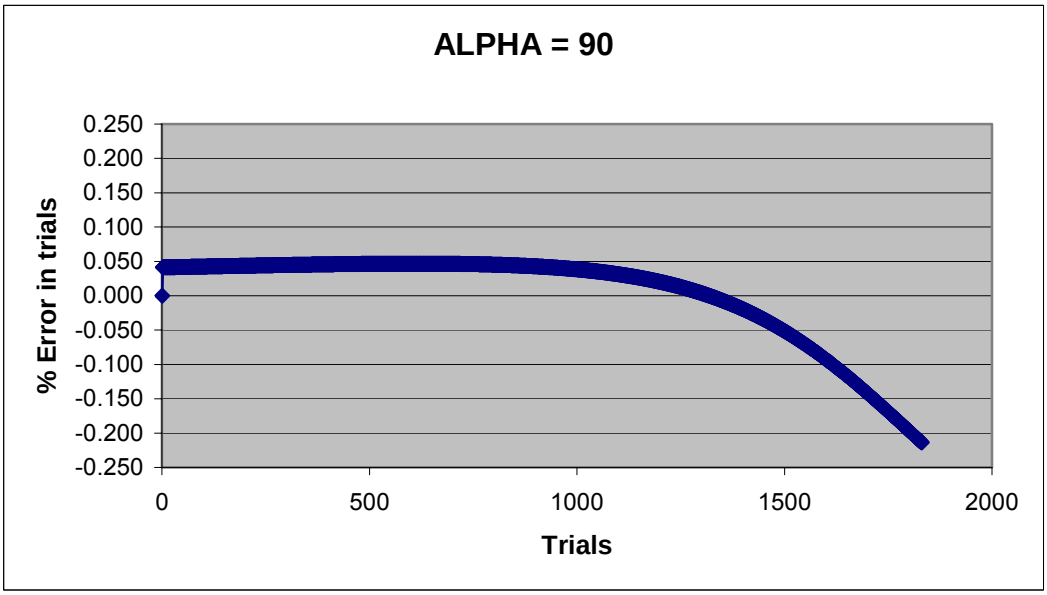

Figure 31. %Error vs. ALPHA for ALPHA =90

The next value for ALPHA was 80, results are shown in Figure 32. It had a much steeper curve than the previous one. It showed that we had now reached a value of ALPHA for which the number of iterations required to obtain the desired value of error was 213, a value much less than the previous ones.

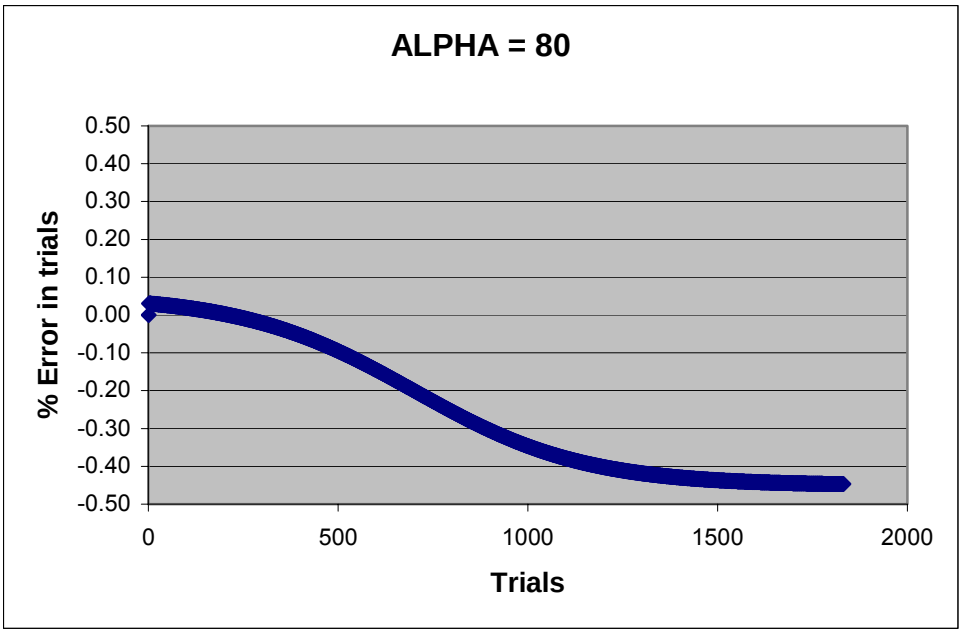

Figure 32. %Error vs. ALPHA for ALPHA =80

The next Figure was plotted with ALPHA equal to 70. Figure 33 shows that the error does not converge but the arrow begins to stabilize to a value less than the desired one. From these trails, it can be concluded that the required ALPHA value lies somewhere between 70 and 80. This was in agreement with Figure 27.

Figure 34 with ALPHA equal to 60 does not converge towards desired value of error. This value of ALPHA and also some subsequent lower ones were taken to check whether the error value happened to converge again. Apparently it was not the case. At the value of initial ALPHA where initial force is maximum, the error value tends to

converge quickly in a few iterations itself. Values which are too high or too low when compared to the value will result in the solution taking longer to converge.

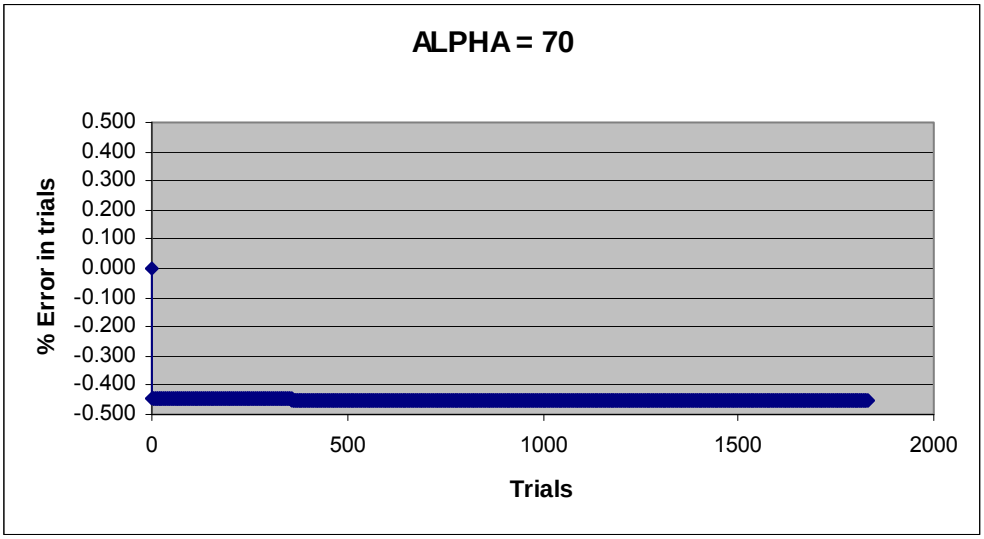

Figure 33. %Error vs. ALPHA for ALPHA =70

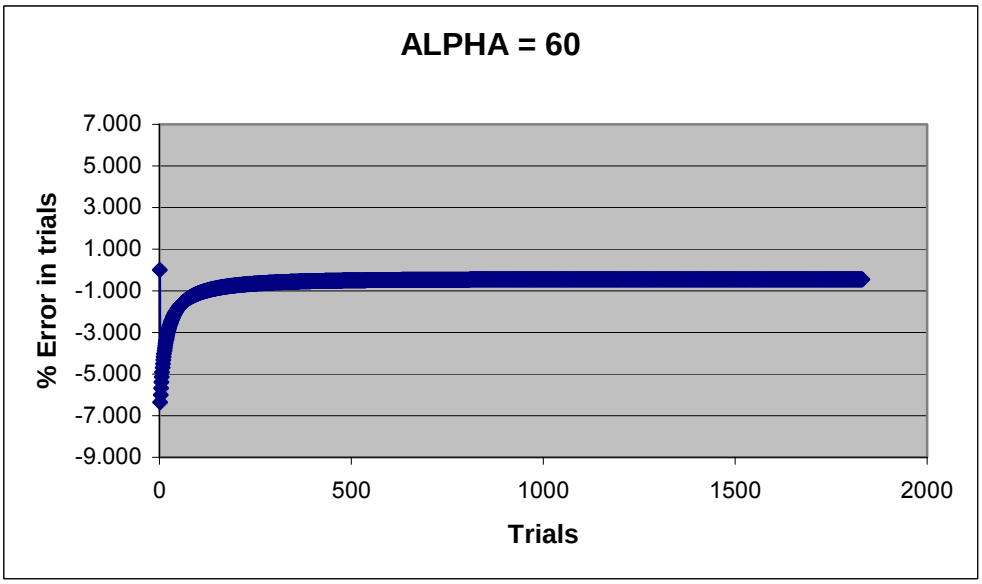

Figure 34. %Error vs. ALPHA for ALPHA =60

Table 6 summarizes the tabulated results from which the figures have been plotted.

Table 6. Conclusive results from the plotted figures

ALPHA initial	ALPHA final	Force initial (Nn)	Force Final (nN)	% Error Final	Trials
92	77.5418072	6.89588163	3.64378209	5.85E-05	1632
90	77.5388358	6.89588036	4.10646827	0.00000559	1320
88	77.5439825	6.89588197	4.61003017	0.00009714	1050
86	77.5467238	6.8958817	5.14498461	0.00014584	809
84	77.5395931	6.89588077	5.69163884	0.00001907	593
82	77.5397062	6.89588083	6.21358326	0.00002109	396
80	77.5501153	6.89588028	6.64730072	0.00020604	213
79.9	77.5406068	6.89588123	6.66499141	0.00003711	205
79.8	77.5431331	6.89588189	6.68219059	0.00008204	196
79.7	77.5459217	6.89588186	6.69888084	0.0001316	187
79.6	77.5489632	6.89588089	6.71504427	0.0001856	178
79.5	77.5404848	6.89588118	6.73066255	0.00003494	170
79.4	77.5440039	6.89588197	6.74571691	0.00009752	161
79.3	77.5477473	6.89588139	6.76018804	0.00016402	152
79.2	77.5399415	6.89588094	6.77405621	0.00002527	144
79.1	77.5441036	6.89588197	6.78730113	0.00009929	135
79	77.5484598	6.89588112	6.79990203	0.00017666	126
78.9	77.541236	6.89588146	6.81183761	0.00004831	118
78.8	77.5459487	6.89588185	6.82308602	0.00013208	109
78.7	77.5390599	6.89588049	6.83362486	0.00000958	101
78.6	77.5440855	6.89588197	6.84343118	0.00009897	92
78.5	77.5492506	6.89588075	6.85248144	0.0001907	83
78.4	77.5427801	6.89588184	6.86075149	0.00007577	75
78.3	77.5481891	6.89588123	6.86821661	0.00017186	66
78.2	77.5419384	6.89588166	6.87485143	0.0000608	58
78.1	77.5475426	6.89588146	6.88062996	0.00016038	49
78	77.5414618	6.89588153	6.88552553	0.00005232	41
77.9	77.5472099	6.89588157	6.88951083	0.00015447	32
77.8	77.5412464	6.89588146	6.89255786	0.00004849	24
77.7	77.5470845	6.8958816	6.89463792	0.00015225	15
77.6	77.5411829	6.89588144	6.89572157	0.00004736	7
77.544016	77.5322525	6.89587427	6.89588197	-0.00011171	1

The highlighted value of initial ALPHA is the value at which initial force is maximum as shown in Figure 34.

5.4. Conclusions

Adhesion of a particle to wafer surface is one of the major problems in the CMP process. This adhesion process is dominated by the van der Waals force present in the vicinity of the particle and surface. Using the theory of elasticity we were able to analyze the vertical displacement of deflection at the mid-point of a surface. The van der Waals force was evaluated as a function of separation distance. We found that van der Waals forces will no longer attract as the distance reached a critical value of ALPHA. This result was shown by the stabilize plot of error % and the number of trials for ALPHA range from 70 to 80.

The successful adoption of elasticity theory to nanoparticle-surface interaction brought insight into CMP. The model tells us that it is not always the case that as the separation distance is decreased, the attraction force will be increased. The force value estimated can be used for slurry design and CMP process estimation.

CHAPTER VI

CONCLUSIONS AND RECOMMENDATIONS

6.1. Conclusions

Adhesion of a particle to wafer surface is one of the major problems in the CMP process. Mechanisms during CMP and post-CMP cleaning using experiments are combined with numerical analysis, and the adhesion process is dominated by the van der Waals force present in the vicinity of the particle and surface.

Results showed that although surfactant molecules can reduce the adhesion between particles, mechanical removal is only effective for a certain sized large particles. For larger particles, cleaning with higher concentration of surfactant and higher operating temperature proved to be effective in reducing the size of residual particles adhere to the substrate surface. Once the particle size reaches a critical size, the remaining small particles will not be removed effectively.

For remaining small particles, adding surfactant can effectively remove the particles. The surfactant has two basic effects. One is to weaken the bonds between particles and particles and surfaces. The other is to prevent further adhesion between particles and wafer surface. The mechanisms were dominated by interfacial interactions. Moreover, using the theory of elasticity we were able to analyze the vertical displacement of deflection at the mid-point of a surface. The van der Waals force was evaluated as a function of separation distance. We found that van der Waals forces will no longer attract as the distance reached a critical value of ALPHA. This result was shown by the stabilize plot of error % and the number of trials for ALPHA range from 70 to 80.

6.2. Recommendations for future work

In order to prevent particulate contamination on the wafer surface, some steps should be taken into considerations. The recommended steps are:

- Modification of the slurry mechanical property for a have high removal rates, excellent global planarity, good surface finish, and low residual contamination. Slurry particles also need to retain its angularity in order to have effective particle contact area, which will lead to uniform planarization.
- During cleaning some loose particles from the brush sweeping may form flocs or particle agglomerates at high surfactant concentration. If the particles agglomerates are triggered by the surfactant in the solution, flocs can be stabilized by adding a micelle breaking agent, such as urea, ethanol, and trichloroacetate in the cleaning solution.
- Since the post-CMP cleaning requires cleaning chemistries modification in order to balance the solution pH and the surface charges of particles and substrate. There needs to be an understanding of electrochemistry and the colloid science principles which will ultimately be beneficial in understanding the post-CMP cleaning process.
- Further study on different types of surfactant will aid in improving the surface integrity. The interaction between different types of surfactant with the slurry particles can be analyzed in order to see the monolayers or bilayers formation on the interface. Finally, the variety of these phase behavior of surfactants in solution can further be encompassed by constructing a phase diagram. These phase diagram will serve as a guide on how much surfactant concentration should be added in order to facilitate effective particle removal.

NOMENCLATURE

P	Applied load
E	Elastic modulus
a	Contact radius
R	Radius of sphere/particle
$\Delta\gamma$	Work of adhesion
K	Composite young's modulus
υ	Poisson's ratio
P_c	Critical force required to separate two spheres
a_0	Contact radius at zero load
D	Diameter of sphere
W_a	Work of adhesion
Y	Yield strength of the yielding material
M	Material's hardness
F_t	Total adhesion force
F_{vdw}	Van der Waal's force
F_{edl}	Electrical dual layer force
A	Hamaker constant
r	Separation distance between the particle and surface
A_r	Real contact area of polishing interface

A_n	The nominal contact area of polishing interface
η	The area density of asperities
R_a	The average radius of the asperities
z	The height of asperity measured from the mean of asperity heights
d	The distance between the rigid flat surface of the wafer and the mean plane of the pad asperities
$\varphi(z)$	Distribution function of the asperity heights
ω	Interference
ω_e	Critical interference at the point of initial yielding of the asperity
ω_p	Critical interference at the point of fully plastic flow
F_r	The contact force at the polishing interface
E'	The equivalent Young's modules for the contact surfaces
H_p	The hardness of the polishing pad material
k	The mean contact pressure factor
A_{pw_total}	Total contact area of the pad asperity/wafer contact
A_{aw_total}	Total contact area of the abrasive abrasives/wafer contact
D	Diameter of particle
δ_{ap}	The penetration depth of abrasive/pad contact interface
δ_{aw}	The penetration depth of abrasive/wafer contact interface.
F_{ap}	The contact force of the pad asperity and the abrasive contact

E_{ap}	The equivalent Young's modulus of polishing pad and abrasive
F_{aw}	Contact force for a single effective abrasive at the wafer/pad asperity contact
H_w	Hardness of the wafer surface
A_{aw}	The contact area for the single effective abrasive of the abrasives/wafer contact
s	Shear strength
F	Friction force
p	Surface roughness angle
r_p	Radius of penetration
R_m	Actual radius of micelle
Rg	Radius of gyration
U	Lennard-Jones potential
B, C	Lennard-Jones potential parameter
F_{lj}	Lennard-Jones force
ALPHA	Dimensionless parameter
F_{i+1}	Iteration force
F_i	Initial force
ε_{rr} , $\varepsilon_{\theta\theta}$, $\varepsilon_{r\theta}$	Corresponding strain in Polar direction
u	Displacement in radial direction
v	Displacement in tangential direction
$\sigma_{\theta\theta}, \sigma_{rr}, \sigma_{r\theta}$	Corresponding stresses in Polar direction

G	Shear modulus
q	Intensity
v_a	Vertical displacement of surface at the mid-point
σ, ε	Lennard-Jones parameters

REFERENCES

[1] J.M. Steigerwald, S.P. Murarka, and R.J. Gutmann, *Chemical Mechanical Planarization of Microelectronics Materials*, John Wiley, New York (1997)

[2] M.R. Oliver (editor), *Chemical Mechanical Planarization of Semiconductor Materials, Springer*, Berlin (2004)

[3] H. Liang, D. Craven, *Tribology in Chemical-Mechanical Planarization*, CRC Press, Boca Raton, FL (2005)

[4] M.J. Rosen, *Surfactants and Interfacial Phenomena*, Wiley-Interscience, Hoboken, NJ (2004)

[5] E. Estragnat, G. Tang, S. Jahanmir, P. Pei, J.M. Martin, H. Liang, *J. Electronic Materials*, **33**, 4 (2004)

[6] E. Estragnat, D. Ng, M. Kulkarni, D. McMullen, K. Bahten, H. Liang, *Controlled Environments Magazine*, **8**, 14 (2005)

[7] K. Kimball, J. Greene, *Cadence Expands Technology Leadership at 0.13-micron-and-below with acquisition of Simplex,* Cadence Press Release, San Jose, CA, April 24, 2002

[8] H. Hertz, J. Reine, *Angew. Math.,* **92**, 156 (1882)

[9] B.V. Derjaguin, V.M. Muller and Yu. P. Toporov, *J. Colloid Interface Sci.* **53**, 314 (1975)

[10] B.V. Derjaguin, V.M. Muller and Yu. P. Toporov, *J. Colloid Interface Sci.* **67**, 378 (1978)

[11] K.L. Johnson, K. Kendall, A.D. Roberts, in *Proc. R. Soc. London*, **A324**, 301 (1971)

[12] D. Maugis, B. Gauthier-Manuel, in D.S. Rimai, L.P. Demejo, K.L. Mittal (editors), *Fundamental of Adhesion and Interfaces*, VSP, Utrecht (1995)

[13] D. Maugis, H.M. Pollock, *Acta Metall.*, **32**, 1323 (1984)

[14] D. Maugis, *J. Colloid Interface Sci.*, **150**, 243 (1992)

[15] B.V. Derjaguin, L.D. Landau, *Acta Physica*, **14**, 633 (1933)

[16] E.J.W. Verwey, J.G.T. Overbeek, *Theory of Stability of Lyophobic Colloids*, Elsevier, New York (1948)

[17] C. Tanford, *The Hydrophobic Effect*, Wiley, New York (1980)

[18] K.A. Dill, P. Flory, in *Proc. Natl. Acad. Sci.*, **78**, 676 (1981)

[19] K. Shinoda, *Solvent Properties of Surfactant Solutions*, Marcel Dekker, New York (1967)

[20] J.H. Fendler, E.J. Fendler, *Catalysis in Micellar and Macromolecular Systems*, Academic Press, New York (1975)

[21] M.J. Schick (editor), *Nonionic Surfactants*, Marcel Dekker, New York (1967)

[22] E. Jungermann (editor), *Cationic Surfactants*, Marcel Dekker, New York (1970)

[23] W.M. Linfield (editor), *Anionic Surfactants*, Marcel Dekker, New York (1973)

[25] K.L. Mittal (editor), *Micellization, Solubilization and Microemulsions*, Plenum Press, New York (1977)

[26] K.L. Mittal (editor), *Solution Chemistry of Surfactants*, Plenum Press, New York (1979)

[27] K.L. Mittal, E.J. Fendler (editors), *Solutions Behavior of Surfactants: Theoretical and Applied Aspects*, Plenum Press, New York (1982)

[28] K.L. Mittal, B. Lindman (editors), *Surfactants in Solution*, Plenum Press, New York (1984)

[29] H.E. Eicke, (editors), *Modern Trends of Colloid Science in Chemistry and Biology*, Birkhduser, Basel (1985)

[30] P.L. Luisi, B. Straub, *Reverse Micelles-Technological and Biological Relevance*, Plenum Press, New York (1984)

[31] J.H. Fendler, *Membrane Mimetric Chemistry*, Wiley, New York (1982)

[32] Semiconductor Industry Association, The National Technology Roadmap for Semiconductors, San Jose (1994)

[33] G.M. Burdick, N.S. Berman, S.P. Beaudoin, *J. Nanoparticle Research*, **3**, 455 (2001)

[34] G.M. Burdick, N.S. Berman, S.P. Beaudoin, *J. Electrochem. Soc.*, **150**, G658 (2003)

[35] G. Zhang, G. Burdick, F. Dai, T. Bibby, S. Beaudoin, *Thin Solid Film*, **332**, 379 (1998)

[36] K. Copper, N. Ohler, A. Gupta, S. Beaudoin, *J. Colloid and Interfacial Sci.*, **222**, 63 (2000)

[37] K. Copper, A. Gupta, S. Beaudoin, *J. Colloid and Interfacial Sci.*, **228**, 213 (2000)

[38] K. Copper, A. Gupta, S. Beaudoin, *J. Colloid and Interfacial Sci.*, **234**, 284 (2001)

[39] K. Copper, A. Gupta, S. Beaudoin, *J. Electrochem. Soc.*, **148**, G662 (2001)

[40] K. Copper, S. Eichenlaub, A. Gupta, S. Beaudoin, *J. Electrochem. Soc.*, **149**, G239 (2002)

[41] S. Eichenlaub, K. Copper, A. Gupta, S. Beaudoin, *Solid State Phenomena*, **76-77**, 283 (2001)

[42] S. Eichenlaub, A. Gelb, S. Beaudoin, *J. Colloid and Interfacial Sci.*, **280**, 289 (2004)

[43] F. Zhang, A. Busnaina , *Appl. Phys. A*, **69**, 437 (1999)

[44] Y.K. Hong, D.H. Eom, S.H. Lee, J.G. Park, A. Busnaina, *Electrochemical Soc. Processings*, **21, 19** (2003)

[45] L. Zhang, S. Raghavan, M. Welling, *J. Vac. Sci. Technol.*, **B17**, 2248 (1999)

[46] Y.R. Jeng, P.Y. Huang, *J. Tribology*, **125**, 232 (2003)

[47] Y. Zhao, L. Chang, *Wear*, **252**, 220 (2002)

[48] E. Rabinowicz, *Friction and Wear of Materials*, Wiley, New York (1995)

[49] W. Choi, U. Mahajan, S.M. Lee, J. Abiade, R.K. Singh, *J. Electrochem. Soc.*, **151**, G185 (2004)

[50] E. Matijevic (editor), *Surface and Colloid Science*, John Wiley, New York (1976)

[51] W. Krussel, J. de Larios, J. Zhang, *Solid State Technol.,* **38**, 109 (1995)

[52] K. Bahten, T. Zhang, E. Estragnat, H. Liang, J. Lee, *CMP/MIC*, March 2002

[53] A. Busnaina, H. Lin, N. Moumen, J.W. Feng, J. Taylor, *IEEE Transactions on Semiconductor Manuf.* **15**, 374 (2002)

[54] A. Philipossian, L. Mustapha, *Solid State Phenomena*, **92**, 275 (2003)

[55] C. Huynh, M. Rutten, R. Cheek, H. Linde, *IEEE/SEMI Advanced Semiconductor Manufacturing Conference*, pp.32 (1998)

[56] C.W. Liu, B.T. Dai, C.F. Yeh, *Applied Surface Sci*., **92**, 176 (1996)

[57] P.L. Chen, J.H. Chen, M.S. Tsai, B.T. Dai, C.F. Yeh, *Microelectronic Engineering*, **75**, 352 (2004)

[58] Y. Liu, K. Zhang, F. Wang, Y. Han, *Microelectronic Engineering*, **66**, 433 (2003)

[59] R. Small, M. Peterson, A. Gorman, Z. Chen, *SEMICON China 1998*, April 23, 1998

[60] B.T. Lin, C.S. Chen, W.K. Yeh, S.N. Peng, *IEEE/SEMI Advanced Semiconductor Manuf. Conference*, pp. 362 (2002)

[61] J. Israelachvili, *Intermolecular and Surface Forces*, Academic Press, San Diego (1991)

[62] K.L. Mittal, *Particles on Surfaces*, Plenum Press, New York (1998)

[63] D. Maugis, *Contact, Adhesion and Rupture of Elastic Solids*, Springer, New York (2000)

[64] S.P. Timoshenko, J.N. Goodier, *Theory of Elasticity*, McGraw-Hill, New York (1970)

[65] R. Qiao and N.R. Aluru, in *Proceedings of the International Conference on Computational Nanoscience and Nanotechnology*, pp. 28 (2002)

VITA

Dedy Ng was born and raised in Pontianak, Indonesia. After graduating as valedictorian from Tarakanita II high school in the summer of 1997, Dedy went to Austin Community College in Austin, TX and received his Diploma in engineering in the fall of 1998. Then he transferred to The University of Texas in the spring of 1999 to continue pursuing his interest in mechanical engineering. During his study at The University of Texas, he worked as an undergraduate research assistant in the Mechanical Engineering Department. He also worked as an engineering intern at Applied Materials for one year to gain valuable professional experience. In the spring of 2003, he received his Bachelor of Science in mechanical engineering with honors. From his research and intern experience, he developed a strong interest in materials area which led him into pursuing the opportunity to enter graduate studies in the mechanical engineering field. At Texas A&M University, Dedy works for Dr. Hong Liang in Chemical-Mechanical Polishing (CMP) projects. His projects focus on modeling of nanoparticles removal and surface deflection using theory of elasticity approach, applying the surface chemistry techniques to study the behavior of nanoparticles interaction during CMP and role of surfactant molecules in post-CMP cleaning. He is also an author of one journal publication in ASTM International and a co-author of three journal publications.

Dedy's permanent address follows:
Jl. Citarum Utara No. 12
Pontianak, KALBAR 78117
Indonesia